Journal of Materials Chemistry A

ROYAL SOCIETY OF CHEMISTRY

REVIEW

View Article Online
View Journal | View Issue

Cite this: J. Mater. Chem. A, 2026, 14, 9852

Durability and degradation of Anion Exchange Membranes in water electrolyzers†

Nicholas Carboni, [a] Maria Assunta Navarra, *[ab] Stefano Passerini *[ac] and Jürgen Garche*[d]

Received 8th August 2025
Accepted 24th December 2025

DOI: 10.1039/d5ta06423f

rsc.li/materials-a

Anion Exchange Membrane Water Electrolyzers (AEMWEs) have emerged in recent years as an attractive alternative to Proton Exchange Membrane Water Electrolyzers (PEMWEs) and Alkaline Water Electrolyzers (AWEs) to produce hydrogen, thanks to the possibility of using cost-effective catalyst materials and less expensive and non-fluorinated Anion Exchange Membranes (AEMs). The major drawback of these systems is the limited durability of AEMs because of mechanical, thermal and chemical degradation, which are influenced by the operating parameters (temperature and pressure) of the AEMWE device. Chemical degradation is, especially, the most severe due to the highly alkaline operating environment of AEMWEs. Investigating the causes of these failures is crucial for optimizing the AEM stability. This review focuses on the degradation mechanisms involved and on possible strategies to mitigate them. An overview of the working principles of AEMWEs is provided, together with the state-of-the-art and the main functional properties of AEMs. Also, the most used cationic functional groups and polymer backbones are analysed along with their degradation pathways.

1 Introduction

Given the significant global energy consumption and growing climate concerns, hydrogen (H_2) has emerged as an appealing energy carrier.[1] The production and utilization of hydrogen through energy conversion technologies, such as water electrolysers powered by renewable sources and fuel cells, have received great attention. Recently, the anion exchange membrane (AEM) technology has attracted interest for both fuel cells (AEMFCs)[2,3] and water electrolyzers (AEMWEs),[4,5] offering several advantages over proton exchange membrane (PEM) devices operating under acidic conditions. The possible use of cost-effective materials, such as nickel and other non-noble metals as catalysts[6,7] and the employment of less expensive polymeric AEMs as the electrolyte to replace perfluorinated Nafion, is the most attractive characteristic. While there have been substantial progress and achievements in AEMFC and AEMWE technologies,[8,9] a challenge remains related to the performance of AEM materials, especially in the long term. To meet the operational requirements, further development of AEM materials is necessary, focusing on ionic conductivity as well as chemical, mechanical and thermal stability. Thus, a better understanding of the ion conduction and degradation mechanisms in AEMs is essential for their further development.

A long service life under a wide range of operating conditions is, in fact, a prerequisite for an economical levelized cost of hydrogen (LCOH), as shown by techno-economic model calculations by Titheridge *et al.*[10]

They conclude that degradation in AEMWEs increases cell voltage and shortens stack lifetime, which raises both electricity consumption and maintenance costs, limiting scalability. It also forces conservative operation and adds plant complexity (*e.g.*, minimization of CO_2 intrusion and alkali management), all of which negatively affect system efficiency and economics.

Approaches such as the use of a stable membrane, optimized stack design and optimal operational controls (temperature, start/stop management, and CO_2 exclusion) can extend lifetime and reduce performance decay.

Techno-economic assessments show that halving degradation rates or doubling stack lifetime can substantially lower the levelized cost of hydrogen by cutting both electricity and replacement expenses. Investing in more durable materials or better controls often yields a net cost benefit, since electricity and stack replacements dominate lifecycle costs.

AEMs contain fixed cations on their polymer structures alongside mobile hydroxide counter anions. The ionic conductivity of AEMs is closely linked to their intrinsic structures, particularly the fixed cations' chemistry, the composition of the polymer backbone, and the linkage between these

[a]Department of Chemistry, Sapienza University of Rome, Piazzale Aldo Moro 5, Rome 00185, Italy. E-mail: mariassunta.navarra@uniroma1.it

[b]Hydro-Eco Research Center, Sapienza University of Rome, Via A. Scarpa 16, Rome 00161, Italy

[c]Austrian Institute of Technology (AIT), Center for Transportation Technologies, Giefinggasse 4, 1210 Vienna, Austria

[d]Visiting Professor (May/Jun 2023) at the Sapienza University of Rome, Institute for Theoretical Chemistry, Ulm University, Helmholtzstr. 16, 89081 Ulm, Germany

† In memory of Prof. Bruno Scrosati (August 1937 – November 2024).

components.[11,12] A main problem of AEM materials is their chemical stability, since OH^- is a strong nucleophile; therefore overcoming alkaline degradation of AEMs is not an easy task.

The AEM cations exhibit distinct electrostatic attraction with hydroxide ions, causing a profound impact on AEM conductivity and durability. The latter is mainly determined by the following degradation mechanisms: Hofmann elimination (E2), nucleophilic substitution (S_N2), and rearrangements.[13]

Regarding AEM performance and durability, the polymer backbone plays a key role, since its degradation result in severe damage to the membranes. In fact, the AEM backbone largely determines the mechanical and thermal stability, which is important especially in AEMWEs working in differential pressure mode.

Recent advancements have seen a substantial improvement in AEMWE performance, with current densities often exceeding 1 A cm^{-2}.[14–18] However, state-of-the-art AEMWEs have a relatively short operational life (typically less than 200 hours), leaving the long-term durability challenge unsolved. Furthermore, achieving high performance often relies on platinum group metal (PGM) catalysts and/or the use of a circulating KOH solution. Using pure water with non-PGM catalysts poses challenges, primarily due to the higher cell resistance, but also because of the fast dissolution of the catalyst itself.[19]

In general, water electrolysis is essentially the reverse process of water formation; therefore, AEMWEs and AEMFCs are very similar.[8] Consequently, the functions and challenges of AEMs are analogous in both kind of devices, particularly those regarding ionic conductivity and alkaline stability. Nevertheless, the distinct operational environments of these devices call for some variations in the AEM characteristic properties. AEMFCs require high humidification and necessitate AEMs with rapid water uptake and permeability, favouring thin but mechanically stable AEMs to enable high power densities. On the other hand, AEMWEs require an increased AEM thickness (or stiffness) to withstand differential pressure operation. This results in an elevated resistance of the AEM, which is offset by using low-concentration alkaline electrolytes instead of pure water.

Despite the significant progress achieved in AEMFCs and AEMWEs, a deeper understanding of the degradation mechanisms, to develop more stable AEMs, is necessary. For this purpose, this review provides for the first time a unique and comprehensive overview of the properties and degradation mechanisms of anion exchange membranes, focusing on the most commonly used commercial membranes, cationic functional groups, and polymer backbones. Particular emphasis is placed on the analysis of degradation mechanisms, going through mechanical, thermal, and chemical pathways in detail, while also covering performance degradation arising from the operating conditions. Furthermore, the review discusses various mitigation strategies aimed at enhancing AEM durability, one of the major challenges currently hindering the large-scale commercialization of anion exchange membrane water electrolyzers.

2 AEM water electrolyzers

The main component in the electrolyzer design is the membrane electrode assembly (MEA), which is a layered structure with the membrane sandwiched between two porous transport layers (PTLs), each coated with the anode or the cathode catalysts on the membrane side, as illustrated in Fig. 1. The PTLs provide the effective mass transport of water towards the catalyst layer and gas products away. The MEA is pressed between two nickel or stainless-steel bipolar plates to ensure correct supply of water or electrolyte solution to the electrodes and correct gas management. An electrolyte solution (usually KOH or K_2CO_3) is fed into the device to achieve better ionic conductivity and catalyst activity.[20] Water is reduced at the cathode side and produces H_2 and OH^- through the hydrogen evolution reaction (HER), while for the oxygen evolution reaction (OER), OH^- spontaneously diffuses across the AEM and is oxidized at the anode side. The following equations display the related reactions:[21]

$$\text{Anode: } 4OH^- \rightarrow O_2 + 2H_2O + 4e^-$$

$$\text{Cathode: } 4H_2O + 4e^- \rightarrow 2H_2 + 4OH^-$$

$$\text{Overall: } 2H_2O \rightarrow 2H_2 + O_2$$

At 25 °C, the thermodynamic potential of the overall reaction is about 1.23 V. However, the overpotentials caused by electron transfer, mass transfer, *etc.*, and the ohmic resistances, require greater cell voltages.[20]

AEMWE cell performance is strongly influenced not only by the current and applied potential but also by operating parameters such as feed type, electrolyte solution, cell temperature and pressure.[22] The reaction kinetics are enhanced when the cell is operated at high temperatures, but high pressures, although helpful for the subsequent hydrogen storage, directly raise the open-circuit voltage due to impeded water diffusion within the electrode and membrane.[23] The ohmic potential drop is decreased, and OH^- conduction is enhanced when a basic electrolyte solution is used instead of pure water.[24] The performance of AEMWE cells is also impacted by single-side (water is supplied to either the anode or the cathode) or double-sided (water supplied to both the anode and the cathode)

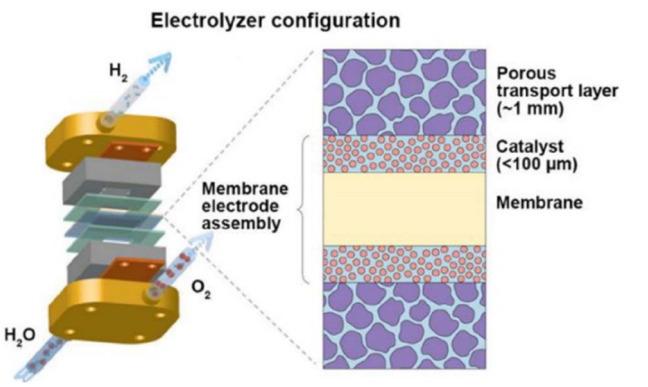

Fig. 1 Schematic of the AEM water electrolyzer and MEA. Reprinted from *Energy Chem.*, vol 4, Xu *et al.*[20], Anion exchange membrane water electrolyzer: electrode design, lab-scaled testing system and performance evaluation, p. 100087, Copyright (2022) with permission from Elsevier.

Table 1 Performance of commercial AEMs.[28]

Membranes	Anode (catalyst loading: mg cm^{-2})	Cathode (catalyst loading: mg cm^{-2})	Temperature (°C)	KOH m olarity (M)	Electrochemical p erformance	Durability	Ref.
Fumasep FAA-3-50	Stainless steel	Pt/C (0.5)	60	1	1.40 A cm^{-2} at 2.0 V	—	29
	$NiFe_2O_4$	Pt/C (0.5)	60	1	1.5 A cm^{-2} at 1.8 V; 2.0 A cm^{-2} at 2 V	~3 mA h^{-1} @ 2 V for 120 h	30
	IrO_2	Pt/C (0.5)	60	1	2 A cm^{-2} at 2.2 V	—	30
	NiO	Pt/C (0.5)	60	1	1.68 A cm^{-2} at 2.2 V	—	30
	IrO_2 (3)	Pt/C (0.5)	60	1	0.6 A cm^{-2} at 1.8 V; 1.2 A cm^{-2} at 2.0 V	1 mA cm^{-2} h^{-1} @ 1.8 V for 120 h	31
	IrO_2 (3)	Pt/C (0.5)	70	1	0.9 A cm^{-2} at 1.8 V; 1.7 A cm^{-2} at 2.0 V	—	31
	IrO_2 (3)	Pt/C (0.5)	80	1	1.05 A cm^{-2} at 1.8 V; 1.2 A cm^{-2} at 2.0 V	—	31
	IrO_2 (2)	Pt/C (2)	60	1	1.0 A cm^{-2} at 2.15 V	~3 mV h^{-1} @ 500 mA cm^{-2} for 8 h	32
	$NiMn_2O_4$	Pt/C (0.5)	80	1	0.53 A cm^{-2} at 2.0 V	120 μV h^{-1} @ 400 mA cm^{-2} for 1000 h (@ 50 °C)	33
	Pt/C (1)	Pt/C (1)	60	0.1	0.03 A cm^{-2} at 2.0 V	~50 μA cm^{-2} h^{-1} @ 2 V for 100 h	34
	Ni foam	Ni foam	60	2	2 A cm^{-2} at 2.65 V	—	35
A201 (Tokuyama)	IrO_2 (Premion®, Alfa Aesar)	Pt/C (Pt 46.5 wt%, Tanaka K. K.)	50	1	1.07 A cm^{-2} at 1.8 V	0.02 A cm^{-2} per voltage cycle at 1.8 V for 1000 cycles (from 1.5 to 2.2 V at a scan rate of 20 mV s^{-1})	36
Aemion™	Commercial nickel felt (75% porous, BEKAERT)	Commercial nickel felt (75% porous, BEKAERT)	60	1	0.5 A cm^{-2} at 2.3 V	2 mV h^{-1} @ 200 mA cm^{-2} for 100 h	6
	IrO_2 (1.5)	Pt/C (0.1)	70	1	1.0 A cm^{-2} at 1.75 V	~5 mV h^{-1} @ 10 mA cm^{-2} for 20 h	37
	NiS_2/Ni_3S_4 (5)	Pt/C (0.8)	60	1	1.5 A cm^{-2} at 2 V	0.12 mV h^{-1} @ 1000 mA cm^{-2} for 500 h	38
Sustainion® X37-50	Stainless steel	Pt/C (0.5)	60	1	2.74 A cm^{-2} at 2.0 V	—	29
	Commercial IrO_2/CP	$Ni@Ni(OH)_2$/Ti	50	1	1.0 A cm^{-2} at 2.0 V	—	39
	NiFe	Ni	40	1	0.3 A cm^{-2} at 2.0 V	1 mV h^{-1} @ 400 mA cm^{-2} for 7 days	40
	IrO_2 (2)	Pt/C (2)	60	1	1.8 A cm^{-2} at 2.0 V	~5 mV h^{-1} @ 1000 mA cm^{-2} for 100 h	41
	$NiFe_2O_4$ (1.8)	RANEY® nickel (2.7)	60	1	0.744 A cm^{-2} at 1.8 V	0.7 μV h^{-1} @ 1000 mA cm^{-2} for 10 100 h	42
	IrO_2/CP	Pt/C/CP (40 wt%, EP40)	50	1	0.96 A cm^{-2} at 1.9 V	—	43
	CuCoO	NiCoO–NiCo/C	60	1	0.504 A cm^{-2} at 1.8 V	2.0 mV h^{-1} 440 mA cm^{-2} for 150 h	44
Orion TM1	IrO_2	Pt/C	70	1	2.75 A cm^{-2} at 1.9 V	55 mV h^{-1}@ 500 mA cm^{-2} for 50 h	5
XION™ c omposite-72-10CL	IrO_x	PtNi	60	0.3	2.48 A cm^{-2} at 2.0 V	5 mV h^{-1} @ 1000 mA cm^{-2} for 50 h	45
PiperION™ (Versogen)	Ni foam (Bekaert)	Pt/C (0.5)	60	1	0.62 A cm^{-2} at 2 V	—	38

Table 2 State-of-the-art and expected AEMWE key performance indicators (KPIs) based on the International Renewable Energy Agency reports.[46,47]

	2020	Target 2050	R&D focus
Lifetime (stack)	>5000 hours	100 000 hours	Membrane, electrodes
Stack unit size	2.5 kW	2 MW	MEA
Electrode area	<300 cm^2	1000 cm^2	MEA
Cold start (to nominal load)	<20 minutes	<5 minutes	Insulation (design)
Capital costs (stack) minimum 1 MW	No estimation available	<USD 100/kW	MEA
Capital cost (system) minimum 10 MW	No estimation available	<USD 200/kW	Rectifier

feeding.[25] In particular, the single-side feed to the anode is advantageous for dry H_2 gas collection at the cathode, eliminating extra processing to separate the produced H_2 from the liquid reactants.

The stability and longevity of the electrolysers should be considered when determining the operating conditions. The polymer backbone or functional groups of a membrane will deteriorate at temperatures over its thermal stability range and this degradation is amplified when a highly concentrated alkali solution is added, resulting in a decline of MEA performance.[26,27] As a result, proper operation is crucial for the stability of the materials used in AEMWE cells as well as the cells' performance. To shed light on the implications for the electrolysis performance, the operating conditions of AEMWEs and their effect on the stability of the AEM will be discussed in Section 5.2.

Table 1 shows the performance and stability data of the most used commercial AEMs for electrochemical water splitting. The evaluated system performance is based on the current density achieved at specific voltages, while durability is the system's ability to maintain stability over extended operational periods. Details on the operating conditions and adopted catalysts are also given.[28]

Currently, the large-scale application of AEMWEs is impeded by the relatively poor durability of the available AEMs. It should be noted that a Sustainion® X37-50 anion exchange membrane has demonstrated the best performance and long-term durability in electrochemical water-splitting systems. Its optimized design, based on a 1,2,4,5-tetramethylimidazole functional group, provides high hydroxide conductivity ($\approx$115 mS cm^{-1} at 60 °C) and good chemical stability in alkaline media.

When paired with Pt/C catalysts, the Sustainion membrane achieved 1.8 A cm^{-2} at 2.0 V, outperforming Fumasep® membranes ($\approx$1.2 A cm^{-2} at the same voltage), underscoring the importance of ionic group chemistry for efficient charge transport. In configurations using $NiFe_2O_4$ anodes and RANEY® Ni cathodes, Sustainion X37-50 exhibited 0.744 A cm^{-2} at 1.8 V for >10 000 h, with a voltage degradation rate of only 0.7 μV h^{-1}.

In contrast FAA-3-50 membranes showed poor durability and high degradation rates not exceeding 1000 hours of operation.

Aemion™, based on methylated polybenzimidazole, achieves high current densities (1.0–1.5 A cm^{-2} at ~2.0 V) but undergoes ring-opening degradation of the imidazolium moiety under alkaline conditions. XION composite membranes exhibit 2.48 A cm^{-2} at 2.0 V with promising mechanical reinforcement but require further long-term validation, and PiperION™, featuring a rigid aryl backbone and piperidinium cations, demonstrated 0.62 A cm^{-2} at 2.0 V (1 M KOH, 60 °C), showing potential though lacking extended durability data. Overall, Sustainion® X37-50 stands out for its balance of high conductivity, alkaline resilience, and extended operational stability, but for all other reported AEMWEs, longevity no longer than 3000 h has been reported, highlighting the need of intensive research before the commercialization threshold of AEMWEs can be reached. Table 2 shows AEMWE state-of-the-art key performance indicators (KPIs) along with the expected ones for 2050.[46,47]

3. AEM

3.1 Membrane structure: backbone

AEMs are typically composed of a polymeric backbone with grafted cationic groups to assure the ionic conductivity. Their stability depends on the chemical structure of both the cationic groups and the polymer backbone.[48]

Numerous polymers have been explored for the application as AEMs in alkaline electrolyzers and fuel cells. For example, poly(-vinyl benzyl chloride) (PVBC),[49] polystyrene (PS),[50,51] poly(vinyl alcohol) (PVA),[52–54] styrene-(ethylene–butylene) (SEBS),[55,56] chlorinated polypropylene (CPP),[57,58] polyether ether ketone (PEEK),[59–61] polysulfone (PSU)[62–64] polyethersulfone (PES),[65,66] polyetherimide (PEI),[67,68] poly(*p*-phenylene oxide) (PPO),[69,70] polybenzimidazole (PBI),[71] and poly(terphenylene),[72,73] among others. The most common polymer backbone structures are shown in Table 3.

The backbone structure affects the aggregation of cationic side groups and hydroxide anions by hydrophilic/hydrophobic regulation; moreover, the cation linkage (different locations of cations along the polymer backbones by graft/comb-shape) and distribution of the microphase morphology act as key factors affecting the properties of AEMs as well. A flexible and long alkyl side chain might be used to manipulate the cation linkage and degree of phase separation, improving the ionic conductivity and alkaline stability.[74] Several factors need to be accounted to design an optimal polymer chain, for example cation strings/clusters tethered to the backbone increase the IEC, free space, and mobility,[75] but cationic groups inserted on pendant electron-donating alkyl spacer sidechains along the backbone have been shown to largely reduce the detrimental elimination reactions, with the steric effects maximized for the alkyl chain's length of four or six carbon atoms.[76] Therefore, constructing a well-connected hydroxide pathway by linkage adjustment is imperative to obtain optimal stability and ionic conductivity.

Table 3 Structure of the most common polymer backbones

Polymer backbone	Structure
Poly (vinyl benzyl chloride) (PVBC)	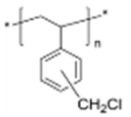
Polystyrene (PS)	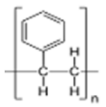
Poly (vinyl alcohol) (PVA)	
Styrene-(ethylene–butylene) (SEBS)	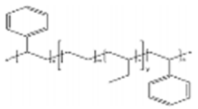
Chlorinated polypropylene (CPP)	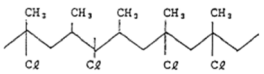
Polyether ether ketone (PEEK)	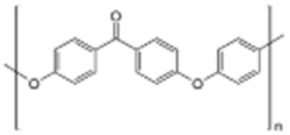
Polysulfone (PSU)	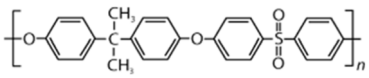
Polyethersulfone (PES)	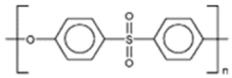
Polyethylenimide (PEI)	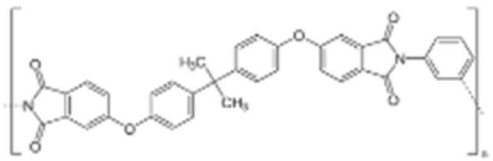
Poly(*p*-phenylene oxide) (PPO)	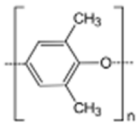
Polybenzimidazole (PBI)	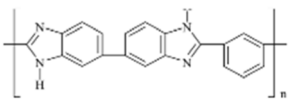
Poly(terphenylene) (PTPN)	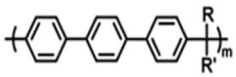

3.2 Membrane structure: cationic functional groups

The cationic functional groups have a strong impact on the ionic conductivity and stability of AEMs.

A variety of cationic groups have been synthesized and studied by experimental and computational investigations, such as quaternary ammonium,[77–80] gemini quaternary ammonium,[81] spirocyclic quaternary ammonium[82,83] imidazolium,[84–86] benzimidazolium,[87,88] pyridinium,[89,90] pyrrolidinium,[91,92] guanidinium,[93–95] pyrazolium,[96] morpholinium,[97,98] 1,4-diazabicyclo-[2.2.2]-octane (DABCO),[99,100] 1,2,3-triazoles,[101,102] piperazinium,[103] methylated melamine,[104] phosphazenium[105,106] and tetrakis(dialkylamino)phosphonium,[106] quaternary phosphonium,[107–109] tertiary sulfonium,[110] triarylsulfonium,[110] and metal cations.[111–113] Table 4 shows the structures of the most common functional groups.

Table 4 Structure of the most common cationic functional groups

Cationic group	Structure
Ammonium-based functional groups	
Quaternary ammonium	
Gemini quaternary ammonium	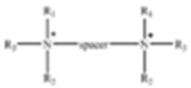
Spirocyclic quaternary ammonium	
Imidazolium	
Benzimidazolium	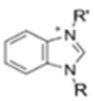
Pyridinium	
Pyrrolidinium	
Guanidinium	
Pyrazolium	
Morpholinium	
1,4-Diazabicyclo-[2.2.2]-octane (DABCO)	
1,2,3-Triazoles	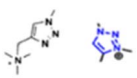
Piperazinium	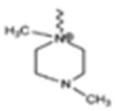
Methylated melamine	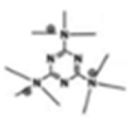
Non ammonium-based functional groups	
Phosphazenium and tetrakis(dialkylamino)phosphonium	
Quaternary phosphonium	
Tertiary sulfonium	

Table 4 (*Contd.*)

Cationic group	Structure
Triarylsulfonium	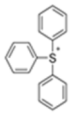
Metal cations (metallocenes, bis(terpyridine) and crown ether complexes)	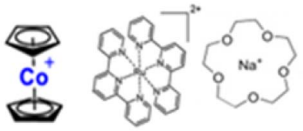

Among the cationic functional groups shown in Table 4, quaternary ammonium (QA) cations have been mostly researched due to their maturity and low cost in synthesis.[114,115]

The major problem of all functional groups is their stability in alkaline environments: the synthesis of highly conductive and stable cations is imperative to develop efficient and effective AEMs and AEMWE devices.

3.3 Commercially available membranes

Anion exchange membranes have been under development for over seven decades.[116] However, due to the low alkaline stability of the earlier membranes, they were predominantly used and optimized for applications in less aggressive environments, such as desalination, electrodeionization, or electrodialysis.[117] While there were early reports on AEM-based fuel cells,[118] research on AEMWEs started relatively late.[25,119] Consequently, even though several membranes have been produced by companies, Table 5 features only a selection of those that have been studied in AEMWEs. Thus, the table does not encompass the properties of all available membranes or membrane grades. Additional membranes are accessible upon request, with variations in thickness, inclusion of a support and/or other enhancements.[120] It should be noted that the comparison of hydroxide conductivity values for AEMs is often unreliable because different measurement procedures are used by manufacturers. For example, Fumatech determines hydroxide conductivity by first immersing membranes in KOH solution to ensure ion exchange, followed by rinsing in pure water to remove excess KOH. However, complete ion exchange is not always achieved, and unless the process is conducted in a closed, CO_2-free environment—such as using nitrogen-purged water or within a glove box—carbonation can occur, lowering accuracy.[121]

An alternative and more precise approach is electrochemical carbonate removal, where a voltage is applied under CO_2-free conditions to purge carbonates from the membrane. Conductivity values obtained through this method are significantly higher and better represent those observed in practical AEM water electrolyzers.[124]

Water permeability, another key membrane property, is often omitted from tabulated data but plays a critical role in system performance. When the electrolyte solution is supplied to both electrodes, water transport through the membrane is less significant since the balance is easily maintained. However, feeding the electrolyte solution only to the anode chamber can be advantageous and it is a very common practice.[36] This mode minimizes gas bubble blockage in catalyst layers, enhances performance, and reduces hydrogen gas humidity, minimizing the efforts to dry the hydrogen.

If water transport from anode to cathode is insufficient, mass transport limitations may arise due to unbalanced hydration or electro-osmotic drag, where hydroxide ions move from the cathode to the anode. Conversely, excessive water crossover can lead to cathode flooding and reduced efficiency. Proper control of membrane hydration is therefore crucial for stable electrolyzer operation.

Mechanical properties are typically reported under controlled laboratory conditions, usually in the dry halide form at room temperature. However, the more relevant wet hydroxide form at elevated temperature is rarely characterized, as it requires inert, humidity-controlled testing environments. Consequently, reported data often fail to represent real operating conditions.

For practical AEM applications, high tensile strength, high Young's modulus, and high elongation at break are desirable. A flexible membrane capable of withstanding mechanical stress without cracking is particularly valuable, as it enhances durability and operational reliability under electrochemical conditions.[120]

4 AEM functional properties

4.1 Introduction

Chemical homogeneity, structure, stability, and mechanical properties are in the main focus of AEM characterization techniques. Analytical techniques such as energy-dispersive X-ray (EDX), nuclear magnetic resonance (NMR), Fourier-transformed infrared (FTIR), and small-angle X-ray scattering (SAXS) are used to characterize the membrane morphology (*e.g.*, pore structure and surface roughness) and molecular distribution (*e.g.*, uniform distribution of head groups and formation of ion clusters).[125] Ion Exchange Capacity (IEC), water uptake, swelling

Table 5 Commercial AEMs and their reported properties

Brand name	Company	Country	Product code	Thickness (μm)	IEC (meq g^{-1})	Ion conductivity (mS cm^{-1})	ASR (Ω cm^2)	Dimensional stability (%)	Tensile strength (MPa)	Elongation at break (%)	Structure
Fumasep® FAA3	Fumatech	Germany	FAA-3-30	25–35[a]	1.7–2.1 (Cl)[a]	4–7 (Cl)[a] 40 (OH)[120]	0.3–0.5 (Cl)[a]	0–2 (Br)[a]	25–40[a]	20–40[a]	Polyaromatic polymer with ether bonds in the main chain, and quaternary ammonium groups attached to the main chain
			FAA-3-50	47–53[a]	1.85[a]	As above	<2.5(Cl)[a]	As above	As above	As above	
			FAA-3-PK-75	75[a]	1.39 (Cl)[a]	>2.5 (Cl)[a]	<2.0 (Cl)[a]	0 (Br)[a]	20–45[a]	30–50[a]	
A201	Tokuyama	Japan	A201	28 (ref. 120)	1.8 (ref. 120)	42 (OH)[120]	Na	2 (MD)[120] 6 (TD)[120]	96 (dry, Cl)[122]	62 (dry, Cl)[122]	Hydrocarbon-based membrane with quaternary ammonium groups
AEMION™	Ionomr	Canada	AF1-HNN8-50-X	50[a]	2.1–2.5[a]	>80[a]	0.13[a]	na	60 (dry, I)[a]	85–110 (dry, I)[a]	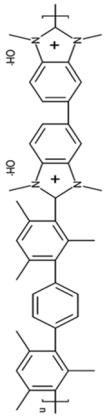
			AF1-HNN8-25-X	25[a]	2.1–2.5[a]	>80[a]	0.063[a]	na	60 (dry, I)[a]	85–110 (dry, I)[a]	
			AF1-HNN5-50-X	50[a]	1.4–1.7[a]	15–25[a]	0.42–0.67[a]	na	60 (dry, I)[a]	85–110 (dry, I)[a]	
			AF1-HNN5-25-X	25[a]	1.4–1.7[a]	15–25[a]	0.21–0.33[a]	na	60 (dry, I)[a]	85–110 (dry, I)[a]	
Sustainion®	Dioxide materials	USA	Sustainion X37–50	50 (ref. 123)	na	80 (1 M KOH, 30 °C)[123]	0.045 (1 M KOH)[123]	Cracks when dry	Cracks when dry	Cracks when dry	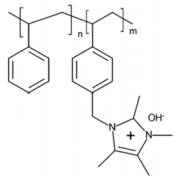
Orion TM1	Orion polymer	USA	Pure material *m*-TPN1[72]	24 (ref. 72)	2.19(OH)[a]	19 (Cl)[72] 54 (OH)[72] >60[a]	na	6 (Cl)[72] 10 (OH)[72]	30 (ref. 72)	35 (ref. 72)	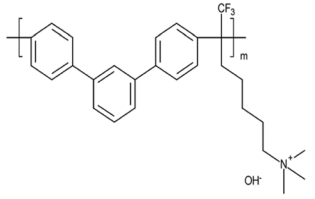

Table 5 (*Contd.*)

Brand name	Company	Country	Product code	Thickness (μm)	IEC (meq g^{-1})	Ion conductivity (mS cm^{-1})	ASR (Ω cm^2)	Dimensional stability (%)	Tensile strength (MPa)	Elongation at break (%)	Structure
XION™	Xergy Inc	USA	XION™ composite-72-10CL	10[a]	3.4–3.6[a]	na	na	na	na	na	
PiperION®	Versogen	USA	PiperION® self-supporting	20–80[a]	2.35 [a]	150 (OH, 80 °C)[a]	na	na	>30–50[a]	>20–100[a]	

[a] From the technical data sheet.

ratio, contact angle, conductivity, and alkaline stability measurements are commonly used to evaluate AEMs' performance and chemical stability;[117,126] tensile strength, elongation at break and dimensional stability tests are used to evaluate AEMs' mechanical properties while thermogravimetric analysis (TGA) and differential scanning calorimetry (DSC) are helpful to determine AEMs' thermal stability.[127]

4.2 Ionic exchange capacity

The ionic exchange capacity is a measure of the number of exchangeable ions per membrane dry weight (meq g^{-1} or mmol g^{-1}).[125] IEC determination procedures for AEMs are not as well defined as those for PEMs. IEC can be evaluated using a variety of techniques, such as titration, spectroscopy (UV-vis), and ion selective electrodes (such as pH probes) to quantify the amount of H^+/OH^- ions in a solution.[128] The most popular techniques are titration methods, such as the Mohr method or acid/base titration.

The approach for the acid/base titration consists of soaking the AEM in a strong base solution (such as 1 M NaOH) to convert it into the OH^- form. Following, the AEM is soaked in a strong acid (*e.g.*, HCl) solution with a known volume and concentration to convert it into the Cl^- form. The resulting diluted HCl solution is then titrated with standardized NaOH to the phenolphthalein endpoint after the AEM is removed and rinsed with DI water.[129]

The Mohr approach involves soaking an AEM in a salt solution (such as 1 M NaCl) to transform it into the Cl^- form. To help with the release of Cl^-, the AEM is then washed and equilibrated in a 0.5 M Na_2SO_4 solution. The AEM/Na_2SO_4 solution is titrated until the K_2CrO_4 endpoint, which indicates that all chlorides have precipitated and Ag_2CrO_4 is currently forming, using an $AgNO_3$ solution with K_2CrO_4 as the indicator.[130]

Achieving high ion-exchange capacity is important to maximize hydroxide conductivity in anion exchange membranes, as more cationic sites provide efficient ion transport pathways. However, increasing IEC typically raises water uptake and swelling, weakening mechanical strength and exposing the polymer to chemical degradation. This leads to a core trade-off: higher IEC improves conductivity but compromises alkaline stability.[75,125,131]

To mitigate this conflict, several strategies have been proposed, such as the use of chemically robust cations and ether-free backbones[131] or controlled crosslinking and hydrophobic–hydrophilic phase separation, which can limit swelling while maintaining efficient ion channels.[132]

Additionally, developing AEMs with cationic sites separated from the main chain shields the backbone from hydroxide attack, balancing IEC and durability. Optimizing membrane morphology and hydration enables high conductivity at moderate IEC levels, achieving both performance and durability.[133,134]

4.3 Water uptake

The water uptake (W.U.) is the change in the membrane mass in response to water exposure. It is measured as described in ref. 135, and it is defined as:

$$\text{W.U.}(\%) = \frac{m_{\text{wet}} - m_{\text{dry}}}{m_{\text{dry}}} \times 100$$

Here, m_{wet} is the weight of the membrane after water exposure at a certain temperature, and m_{dry} is the weight of the AEM after drying.

4.4 Swelling ratio

The swelling ratio (S.R.) is a measure of the linear expansion of the membranes when exposed to water[136] and is calculated as:

$$\text{S.R.}(\%) = \frac{l_{\text{wet}} - l_{\text{dry}}}{l_{\text{dry}}} \times 100$$

Here, l_{wet} is the thickness of the membrane after water exposure at a certain temperature and l_{dry} is the thickness of the AEM after drying.

4.5 Membrane water content

The membrane water content (γ) is related to the number of water molecules per mobile ion and is determined by dividing the water uptake by the molecular weight of water and the IEC.[137]

The W.U. is multiplied by 10 to account for the fact that the IEC is provided in mmol g^{-1}, while the W.U. is reported in percentage:

$$\gamma = \frac{10 \times \text{W.U.}}{m_{\text{H}_2\text{O}} \times \text{IEC}} \times 100$$

4.6 Hydroxide conductivity

The hydroxide conductivity (σ) can be measured in a two- or four-electrode testing cell by using electrochemical impedance spectroscopy (EIS).[138] An AEM is fixed in the testing cell, and a varied AC current is provided to gather impedance data after the AEM has been soaked in DI water or KOH solution for the entire night. The membrane ionic resistance (R_{m}) can be determined by nonlinear least squares regression analysis, and the conductivity can then be calculated using the following formula:[139]w

$$\sigma = \frac{L}{R_{\text{m}} \cdot A}$$

here L is the distance between the electrodes, and A is the cross-sectional area perpendicular to the current flow.

To measure the OH^- conductivity of AEMs without the contribution of carbonate (CO_3^{2-}) and bicarbonate (HCO_3^-) ions, which can affect the measurements, Dekel *et al.*[124,140] proposed a decarbonation method prior to the conductivity test that consists of applying a direct current of 100 μA *in situ* to the AEMs until a stable conductivity value is reached.

4.7 Water contact angle

The water contact angle (θ) is related to the membrane surface's wettability. Large contact angles signify highly hydrophobic surfaces. The sessile-drop technique can be used to measure this parameter.[141]

4.8 Alkaline stability

The alkaline stability is a measure of how the AEM's performance and properties vary under high-pH conditions over time.[135] Although testing settings differ, the general approach is to soak the AEM in a high-pH solution (such as 1–10 M KOH) at a specific temperature (either room temperature or increased temperature) over extended times, periodically testing the membrane IEC and/or conductivity. To evaluate alkaline stability at various hydration levels, Dekel *et al.*[80] suggested an alternative *ex situ* alkaline stability test employing NMR and a water-free hydroxide (crown ether/KOH) solution. This allowed for control over the water/OH^- ratio (γ), as it has been shown that alkaline stability is influenced by the hydration level of the nucleophile (OH^-).

4.9 Mechanical and thermal properties

Thermal stability, tensile strength, elongation at break, and stress–strain curves are measured to evaluate AEMs' thermal and mechanical properties. Thermogravimetric analysis and differential scanning calorimetry are used to assess the thermal stability of the membrane, which is crucial given the working temperatures of AEMFCs (up to 200 °C) and AEMWEs (usually 50–70 °C).[142]

To evaluate the membrane's thermal stability, TGA yields the temperatures at which weight changes occur, resulting from water losses, head group decomposition, and/or polymer decomposition.[143] Besides crystallization and melting features, DSC can be used to assess changes in polymer crystallinity and cross-linking, glass transition temperature and the effects of thermal cycling.[144] A universal testing machine can be adopted to stretch membrane samples to measure tensile strength, elongation at break, and stress–strain curves.[144,145]

Several, but not all, of the mentioned parameters can be found as target specification for AEMs in Table 6 based on a recent EU Horizon 2020 call for proposals.[146] These should be viewed not as universally acknowledged benchmarks, but rather as guidelines, noting that a low performance in one parameter might be offset by superior performance in another. For instance, high stability is preferred over high efficiency, but low stability or low ionic conductivity could be offset by small membrane thickness.

Notably, the targets did not include any reference to gas permeation, even though hydrogen crossover is a widely recognized key performance indicator. That is because the area-specific resistance target value in combination with the concentration value of 2% H_2 in O_2, which is the limit for safe operation, indirectly controls the maximum permitted permeability.[120]

5 AEMWE performance degradation

5.1 Overview

The main degradation mechanisms of AEMWE cells are related to the catalyst and the AEM/ionomer.

Catalyst degradation (dissolution, detachment, migration, and agglomeration) occurs at both the anode and cathode side.

Table 6 Target specifications for AEMs determined in the NEWELY project, based on the call conditions (EU Horizon 2020/fuel cells and hydrogen joint undertaking (JU), call FCH-02-4-2019). ASR = thickness/ion conductivity

Parameter	EU target values
Ion conductivity	>50 mS cm^{-1}
Area-specific resistance (ASR)	≤0.07 Ω cm^2
Stability	≤0.07 Ω cm^2 after 2000 h real or simulated operation in an electrolyzer
Tensile strength	>15 MPa
Elongation at break	>100%
Dimensional stability	≤1% in machine direction ≤4% in transverse direction

This is related to a relatively poor interaction between the catalyst-supporting material and the catalyst itself, which can be worsened further by the low chemical stability of some transition metal (Ni, Fe and Co)-based catalysts and noble metal (Ir and Ru) catalysts,[147,148] as well as by the oxidation of the support material, *e.g.*, carbon at the anode.[149]

For more information about the catalyst degradation, please see Section 5.3.2.

The degradation of the AEM/ionomer has different causes – see Fig. 2.

The chemical/electrochemical degradation is related to the alkaline environment and radical attacks; thermal degradation relates to melting and glass transitions as well as hotspots; mechanical degradation occurs mainly *via* swelling or local imperfections in the AEM. For more information about AEM/ionomer degradation, please see Section 5.3.1.

At the anode, the electrochemical/chemical attack on the membrane and the ionomer is particularly strong due to the high electrode potential. Based on the high instability of the ionomer, the catalyst, which is dispersed with soluble anion-conducting ionomers, will degrade. In addition, there are various anions that accumulate on the catalyst surface of the anode, which leads to reduced catalyst activity.

On the cathode side, the degradation of the AEM/ionomer is less severe because of the lower electrode potential. However, a relatively high degradation of the catalyst activity is observed especially if the electrolyte-feed contains contaminants (*e.g.*, Mg^{2+}, Ca^{2+}, and Ni^{2+}), which could plate as metal on the catalyst or precipitate as hydroxide on the catalyst because the pH strongly increases at the catalyst surroundings during the hydrogen evolution reaction.[150] The metal plating and/or the hydroxide deposition cover the catalyst surface leading to both the catalyst activity reduction and mechanical stress caused by the volume increase. Anion contaminants (Cl^- and Br^-) may also be involved in the anodic faradaic reaction because their oxidation potential is in a similar region to the oxidation potential of OH^-.[151]

In Fig. 3, the anode and cathode degradation phenomena are illustrated.

It should be mentioned that, depending on the operating conditions, the dominance of the individual mechanisms discussed above may change. The supporting electrolyte may have a strong influence. Additional electrolyte feeds (*e.g.*, KOH or K_2CO_3) are commonly used to externally establish a high pH environment around the catalyst, leading to high catalyst activity, while increasing the overall ionic conductivity, *i.e.*, enabling high current densities.

5.2 Performance degradation – operating conditions

5.2.1 Temperature and pressure. The impact of operating temperature on the cell's applied voltage at various current densities is shown in Fig. 4a, based on Vidales *et al.*[23] These authors developed a mathematical model that is able to reproduce trends previously observed in the literature and evaluate the performance of AEMWE cells under various operating conditions. As depicted, an increase in temperature results in a decrease of the required thermodynamic reversible potential, as per the Nernst equation, and the enhancement of reaction kinetics, aligning with the predictions of Arrhenius law. These combined effects lead to a lower applied voltage at elevated temperatures, consequently improving performance, which is also the main reason to develop high-temperature solid–oxide electrolyte electrolyzers. This observed trend aligns with findings from other electrolyzer models[152–157] and translates to reduced power consumption for a given hydrogen production rate. Moreover, water electrolysis, being an endothermic reaction, benefits from higher operating temperatures.[156] At elevated temperatures, the kinetics of charge transfer reactions improve, concurrently reducing the Gibbs free energy of the electrochemical reaction. This enhancement in both the electrode reaction kinetics and the energy conversion contributes to increased cell performance.[155] The increase in AEM conductivity with temperature also contributes to that improvement, resulting in a lower ohmic resistance.

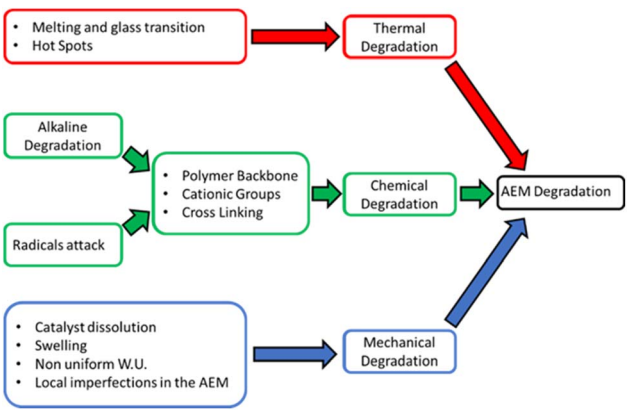

Fig. 2 Principles of the AEM degradation in AEMWEs.

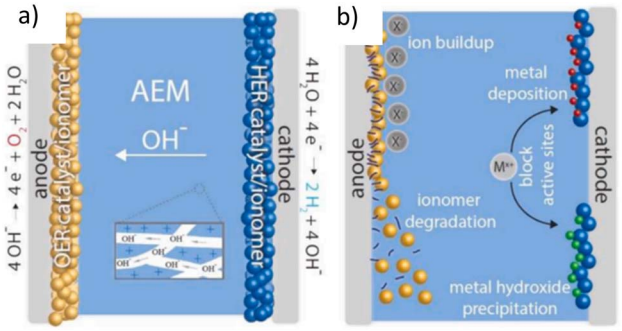

Fig. 3 Degradation phenomena occurring at the anode and cathode of an AEMWE cell: (a) new cell and (b) degraded cell. Reprinted from *Joule*, vol **4**, Lindquist *et al.*,[151] Membrane electrolyzers for impure-water splitting, p. 13, Copyright (2020) with permission from Elsevier.

The other significant operational parameter influencing AEM performance is pressure, significantly impacting the thermodynamically reversible voltage, a relationship described by the Nernst equation. In Fig. 4b, the impact of varying cathode pressures on the AEMWE cell performance is illustrated. While an increase in system operating temperature reduces energy requirements (attributed to the higher temperature aiding the phase change of hydrogen and oxygen products into their gaseous forms), elevated pressure has the opposite effect, resulting in increased cell overvoltage. To explain this, one might consider that the high operating pressure directly raises the open-circuit voltage and may impede water diffusion within the electrode and membrane, thereby increasing diffusion losses.

Fig. 4c shows temperature and pressure plotted against the resulting voltage. The most favourable operational conditions emerge when high temperature is coupled with low pressure.

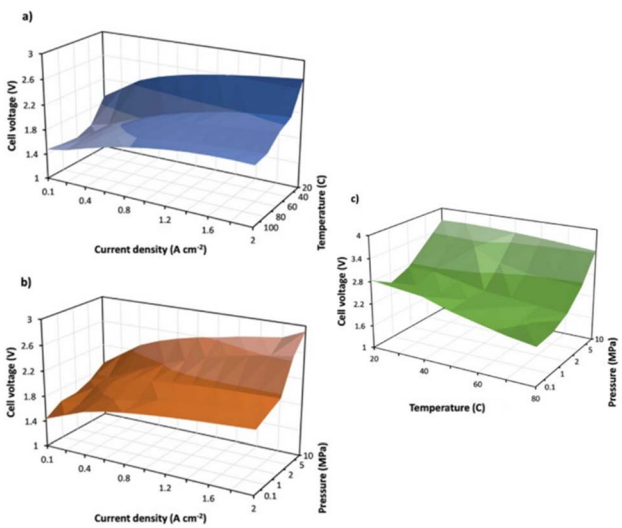

Fig. 4 (a) Effect of temperature on AEMWE performance at constant pressure (1 atm). (b) Effect of pressure on AEMWE performance at constant temperature (60 °C). (c) Combined effects of pressure and temperature on the applied voltage. Reprinted from *Chem. Eng. Res. Des.*, vol **194**, Vidales *et al.*,[23] Modeling of anion exchange membrane water electrolyzers: the influence of operating parameters, p. 13, Copyright (2023) with permission from Elsevier.

This observed behaviour suggests the presence of two opposing effects, resulting in a convex shape. Moreover, it appears that the effect of pressure is less pronounced at high temperatures compared to low temperature, while the influence of temperature is more substantial at higher pressures than at lower pressures. This phenomenon can be elucidated by examining the resulting current density, which rises with increasing temperature due to temperature-dependent kinetics, while it decreases at high pressures.[158] According to the model, the combined effects of temperature and pressure have opposite impacts on AEMWE cells' performance, with the most favourable conditions occurring at high temperatures and low pressures. Specifically, the model identifies the optimal conditions as 75 °C and 1.8 MPa, respectively. These findings align, to a very first approximation, at least as far as the temperature is concerned, with prior research,[152] which suggests an optimal temperature around 60–70 °C and an optimal pressure around 0.2 MPa. However, it must be noted that, according to these previous studies,[152] higher temperatures and/or pressures lead to reduced performance due to electrode degradation and gas crossover, respectively. Thus, achieving optimal electrolysis process performance requires considering the relatively high-pressure values necessary for subsequent hydrogen storage; accordingly, practical electrolyzer working conditions involve a combination of moderate temperatures (40–80 °C) and pressures (1–5 MPa). This strategy aims to both maximize electrolyzer performance and meet the hydrogen storage requirements of the system.[142,159]

5.2.2 Electrolyte medium. An essential operating parameter in AEMWE cells is the electrolyte formulation. Typically, an alkaline solution (such as KOH, usually 0.1–1 M, or 1% wt. K_2CO_3) is introduced into the electrolyzer, but pure water is also an option. However, achieving long-term stable operation with PGM-free catalysts in pure water has proven to be challenging. To ensure stable long-term operation in water-fed AEMWE cells, Ir (iridium) and Pt (platinum) are often employed for the oxygen evolution reaction and, also, the hydrogen evolution reaction. This practice, though effective, contradicts the original intention of replacing costly materials with PGM-free catalysts.[160,161] When PGM-free catalysts are utilized, additional electrolytes, such as KOH, are commonly employed to establish a high pH environment around the catalyst, reducing the overpotential, especially, for the oxygen evolution reaction. Moreover, these supporting electrolytes enhance the system's ionic conductivity, enabling higher current densities.[162]

Mayerhöfer *et al.*[19] and Li *et al.*[163] reported the best performing cells from a literature survey on AEMWE cell performance, employing PGM-free OER catalysts (such as $CuCoO_x$, NiFe and other Ni based electrodes) in different electrolytes. Although the comparison considers different AEM materials, manufacturing strategies, operating temperatures, and variable preconditioning for the MEAs, the survey highlights that operation in KOH solutions (0.1 M–1 M) results in the highest reported performance to date. The current density of the KOH-fed AEMWE cells is, in fact, typically >0.5 A cm^{-2} at 1.6 V, while the current density of the 1 wt% K_2CO_3-fed AEMWE cells is always lower than 0.35 A cm^{-2} at 1.6 V. The pure water-fed AEMWE

cells offer intermediate performance, sometimes reaching 0.5 A cm^{-2} at 1.6 V. Overall, the performance of PGM-free catalyst AEMWE cells follows the trend: concentrated KOH-fed >> pure water-fed > 1 wt% K_2CO_3-fed.

Recently, Krivina *et al.*[164] also demonstrated that some AEMs (*e.g.* PiperION®) degrade more in 1 M carbonate/bicarbonate buffer than in 1 M KOH solution, pointing out that the low conductivity of the carbonate/bicarbonate forms of PiperION® might facilitate a pH gradient leading to oxidative changes in the polymer due to the local pH drop or the absence of sufficient OH^- for the OER.

The durability of pure water-fed AEMWE cells is relatively low.[165,166] The main degradation mechanisms in pure water-fed AEMWEs have been associated with the detachment of the ionomeric binder from the electrocatalysts at the electrodes.[163] This phenomenon is particularly severe with ionomeric binders possessing high ion exchange capacity, which creates high pH environments without the need for an additional circulating liquid electrolyte. Ionomeric binders with high IEC often exhibit substantial dimensional changes under fully hydrated conditions, weakening the adhesion of the ionomer to the catalyst's surface. The lack of adhesion frequently leads to ionomer detachment from the electrode, limiting cell durability. A synthetic approach to ionomers with high IEC and low water uptake may offer a balance between high electrochemical performance and good durability.[167,168] Another durability-limiting factor related to the ionomeric binder is the electrochemical phenyl oxidation.[169,170] The oxidation of phenyl groups in the ionomeric binder results in a rapid voltage jump due to localized pH changes at the electrode occurring relatively quickly. This oxidative process is more detrimental in electrolyzers than fuel cells, given that the operating voltages of the AEMWE anode (1.4–2.2 V) are much higher than those of the AEMFC cathode (0.6–1.0 V). The process begins with the adsorption of phenyl groups of the ionomeric binder onto the catalyst's surface, facilitated by the favourable interaction between the aromatic π-electrons of the phenyl group and the electronic cloud around the metal atoms.[171] The adsorption energy of phenyl group fragments of the ionomer backbone on the Pt surface is even higher than that of benzene.[172] Once adsorbed, the phenyl group undergoes oxidation, converting into phenol. The produced phenolic protons are effectively deprotonated by the hydroxide ions, neutralizing the alkaline medium. Avoiding the presence of phenyl groups in the anode ionomers[173] can solve the issue associated with the electrochemical oxidation of ionomers.

For concentrated KOH-fed AEMWEs, the primary durability-limiting factors differ from those of pure water-fed AEMWEs due to the altered operating environments created by the additional electrolyte. In this case, high IEC ionomers may not be necessary, mitigating the performance loss associated with ionomer detachment. Moreover, the electrochemical oxidation of phenyl groups in the AEM and ionomer becomes less critical because the liquid electrolyte can neutralize the phenols without significantly altering the local pH at the catalyst–electrolyte interface.[163] While circulating a concentrated alkali hydroxide solution enhances AEMWE performance and performance tolerance to ionomer degradation, the corrosive nature of the liquid electrolyte accelerates the degradation of AEMs and other AEMWE components. Consequently, the chemical and electrochemical stability of AEMs becomes a major concern for concentrated KOH-fed AEMWEs.

Lastly, it should be pointed out that the operation mode can also have an impact on the durability: Niaz *et al.*[174] showed that frequently subjecting the cell to rest times without feeding solution may deteriorate the membrane. The solution feeding should be continuous even when the cell is subjected to the rest time. The frequent rest times without solution can, in fact, cause lower humidity levels inside the cell, resulting in irreversible degradation in the membrane.

5.2.3 Carbonation of the membrane. Besides the electrolyte medium itself, the CO_2 load of the electrolyte plays a role in the operation of AEMWEs, leading to performance degradation *via* carbonation of the membrane and the electrolyte.

Carbonation occurs when the cell is exposed to carbon dioxide (CO_2). The primary source of CO_2 is mainly the ambient air. When the cell comes into contact with CO_2 or is supplied with a solution containing CO_2, its reaction with hydroxide anions leads to bicarbonates and carbonates, as illustrated in the following reactions:

$$OH^- + CO_2 \rightleftarrows HCO_3^-$$

$$HCO_3^- + OH^- \rightleftarrows CO_3^{2-} + H_2O$$

However, recent experimental[175–177] and theoretical[178–180] studies have enabled a much more complete understanding of the effects of CO_2 on AEM performance.

Briefly, the mobilities of (bi-)carbonate are lower than OH^-, resulting to an increase in the ohmic resistance of the electrolyte. Parrondo *et al.*[181] demonstrated that short-term performance losses in the system were attributed to CO_2 intrusion, emphasizing the remarkable sensitivity of these systems to CO_2. Its intrusion can lead to the formation of carbonate ions, contributing to increased ohmic resistance: the mobility efficiency of HCO_3^- (4.61×10^{-8} m^2 s^{-1} V^{-1}) and CO_3^{2-} (7.46×10^{-8} m^2 s^{-1} V^{-1}) is, in fact, much lower than that of OH^- (20.64×10^{-8} m^2 s^{-1} V^{-1}) in aqueous solutions.[182] The study revealed that effective electrolyzer cell sealing, to minimize CO_2 intrusion, significantly enhances the short-term stability of water electrolyzers.[183]

The parasitic reactions of CO_2 with the alkaline electrolyte, besides decreasing conductivity and increasing cell voltages, can also cause a range of problems including (bi-)carbonate precipitation, electrolyte pH-drift and carbonation of ionomers, lowering the local pH and reducing the catalytic efficiency (Fig. 5).[184,185]

In an anion exchange membrane, bicarbonate, carbonate, and hydroxide ions will be transported to the anode, yielding the following reactions:

$$4HCO_3^- \rightarrow 4CO_2 + 2H_2O + O_2 + 4e^-$$

$$2CO_3^{2-} \rightarrow 2CO_2 + O_2 + 4e^-$$

$$4OH^- \rightarrow 2H_2O + O_2 + 4e^-$$

Martinez-Lazaro *et al.*[186] observed AEMWEs' performance degradation at first and then performance recovery by replacing the KOH solution and/or performing linear sweep voltammetry (LSV). They attributed the performance recovery to (bi-) carbonate's decomposition during cell potential sweeping. Also, Zignani *et al.*[187] found that carbonation phenomena especially occur during shut-down periods. Then, as a new electrolysis cycle begins, carbonate species decompose and release CO_2. This provides a decarbonation method along with the electrolysis process. Since carbonates are dissolved in water, CO_2 release and water circulation that prevents carbonate accumulation are the main sources of the performance recovery. Despite being reversible, carbonation is still one of the factors contributing to the decline in electrolyzer performance. It is recommended that the MEAs' ion exchange procedure is carried out in an inert gas atmosphere prior to electrolyzer installation to prevent carbonation from ambient CO_2.[188]

5.3 Performance degradation – materials

5.3.1 Membrane degradation

5.3.1.1 Chemical degradation. The chemical stability of AEMs is a crucial aspect for achieving high performance and sustainability in alkaline solid polymer membranes. Unfortunately, many AEMs exhibit low chemical stability, especially in alkaline environments. Common issues of AEMs are associated with the cation functional groups. Organic cations, in general, are susceptible to various chemical reactions, such as nucleophilic substitution S_N2 at the α-position, ylide formation leading to Sommelet–Hauser or Stevens rearrangements[189–191] and E2 reactions when β-hydrogens are present.[189] N-conjugated cations can also undergo nucleophilic addition to the C=N bonds.[76] Additionally, when oxygen-based nucleophiles react with phosphonium cations, the Cahours–Hofmann reaction may occur to form phosphine oxide.[192] These reactions contribute to the degradation of AEM performance by reducing the concentration of anion-exchange groups, thereby negatively impacting ionic conductivity.[13] The alkaline environment can also lead to the degradation of the polymer backbone *via* hydrolysis,[193] dehydrofluorination[125] and cross linking,[194] depending on the polymer structure. Another type of chemical degradation is attributed to the radicals that form during the operation; in particular, hydroxyl (OH•) and superoxide (OO•) can attack both the backbone and the functional groups.[195]

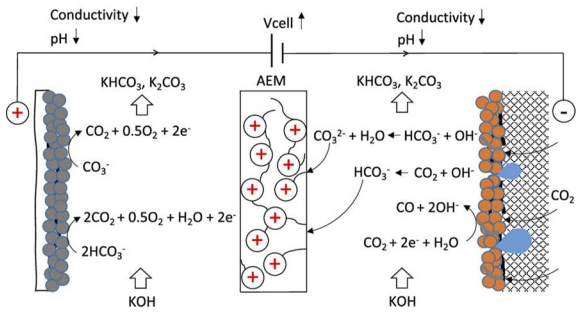

Fig. 5 Illustration of the carbonation problem during electrolysis in a CO_2 electrolyzer, taken as an example. (Bi)carbonates are produced from the reaction of CO_2 with hydroxides and are oxidized at the anode to release CO_2. Adapted from Ramdin *et al.*[184] with permission from American Chemical Society.

5.3.1.1.1 Alkaline degradation of functional groups. The degradation of the cationic functional groups is one of the major problems of AEMs, especially when the electrolyzer is fed with KOH solution. OH^- is a strong nucleophile that can attack positively charged sites, remove protons and add to double bonds.

Fig. 6 depicts the various degradation pathways of the cationic functional groups: (a) S_N2 benzyl substitution,[196] (b) S_N2 methyl substitution,[196] (c) β-elimination substitution,[197] (d) ylide-formation that can lead to Sommelet–Hauser and Stevens rearrangements,[198,199] (e) nucleophilic addition and displacement of pyridinium,[200] (f) nucleophilic degradation of guanidinium[94,201] (g) S_N2 methyl substitution of imidazolium,[202] (h) heterocycle deprotonation of imidazolium,[202] (i) nucleophilic addition to the double bond,[8] and (j) phosphine oxidation.[13]

In the case of cyclic ammonium groups, ring opening reactions are also possible, as reported in Fig. 7: (a) ring opening of imidazolium,[202] (b) S_N2 and ring opening of piperidinium, pyrrolidinium and morpholinium,[203] and (c) ring opening of *N*-spirocyclic ammonium ions.[204]

5.3.1.1.2 Alkaline degradation of the polymer backbone. The chemical stability of the AEM backbone is also crucial for advanced AEMWE systems, as the backbone structure and molecular weight significantly influence the mechanical toughness of the resulting membranes. Common reactions involving the polymer backbone include the cleavage of the ether bond (*e.g.*, in polysulfone), the quaternary carbon hydrolysis and dehydrofluorination when fluorinated carbon structures are present[125] (Fig. 8).

Aryl ether cleavage deteriorates the mechanical properties of quaternized poly(arylene ether) AEMs.[206] The degradation mechanism of the aryl ether cleavage reaction is well documented in previous literature.[207–210] In brief, the electron-donating aryl ether group in the polymer backbone becomes destabilized by the presence of a positively charged (electron-withdrawing) ammonium cationic group in proximity of the backbone. Hydrolysis of the ether bond in benzyl ammonium-functionalized polymers and the consequent mechanical degradation of the AEM may occur even before the degradation of the cationic group. This is because the energy barrier for aryl ether cleavage in the benzyl ammonium-functionalized polymer backbone is 85.8 kJ mol^{-1}, which is lower than the energy barrier for α-carbons on benzyl trimethyl ammonium (90.8 kJ mol^{-1}).[211] Addressing and mitigating these chemical degradation mechanisms are essential for maintaining the long-term mechanical and chemical stability of AEMs in alkaline environments.

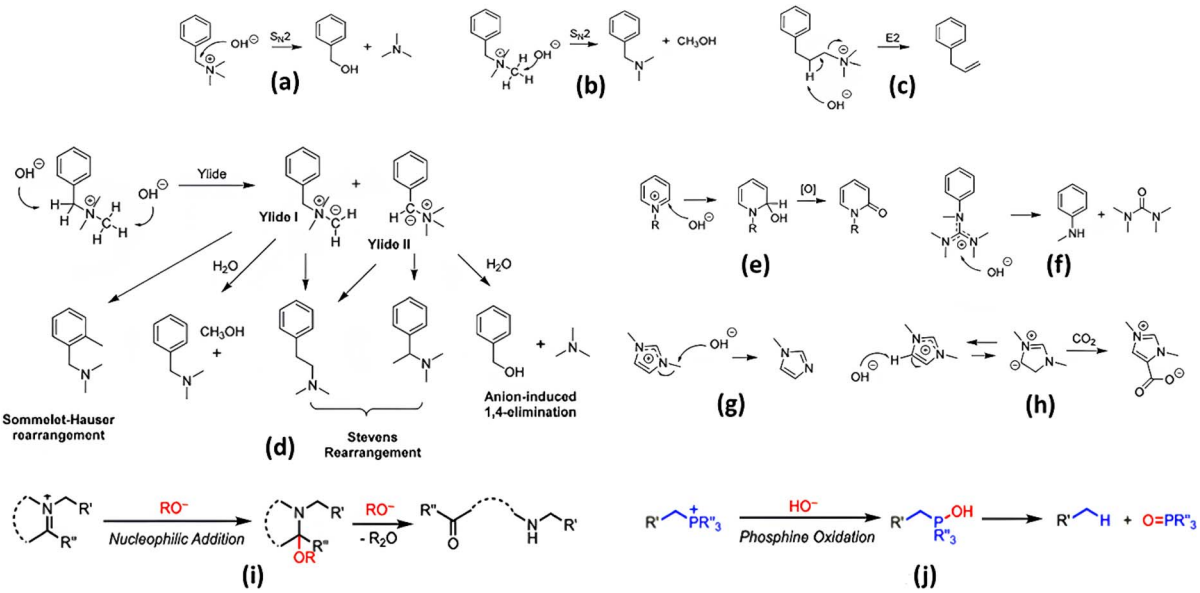

Fig. 6 Degradation pathways of cationic functional groups in an alkaline environment: (a) S_N2 benzyl substitution,[196] (b) S_N2 methyl substitution,[196] (c) β-elimination substitution,[197] (d) ylide-formation that can lead to Sommelet–Hauser and Stevens rearrangements,[198,199] (e) nucleophilic addition and displacement of pyridinium,[200] (f) nucleophilic degradation of guanidinium,[94,201], (g) S_N2 methyl substitution of imidazolium,[202] (h) heterocycle deprotonation of imidazolium,[202] (i) nucleophilic addition to the double bond,[8] and (j) phosphine oxidation.[13] Adapted with permission from You *et al.*[13] (Copyright (2020) American Chemical Society) and Mustain *et al.*[194] (with permission from the Royal Society of Chemistry).

5.3.1.1.3 Cross-linking of AEMs under alkaline conditions. Exposure of AEMs to highly concentrated caustic solutions commonly results in significant gel formation.[212,213] This gel formation arises from cross-linking reactions of quaternized polymers occurring under high pH conditions. While cross-linking reactions are intentionally introduced in AEMs to enhance their mechanical properties,[214–216] uncontrolled cross-linking may lead to undesired property changes of the AEM. The reaction rate of cross-linking depends on the concentration of unreacted alkyl halide, which varies based on the AEM synthetic route. Various cross-linking mechanisms of quaternized polymers under high pH conditions have been identified, such as amine alkylation, Williamson ether synthesis and reactions involving fluorinated backbones[217,218] (Fig. 9). The property changes in AEMs, due to cross-linking reactions, differ from those resulting from chemical degradation. The IEC of AEMs typically changes minimally, as the cross-linking reaction itself does not significantly consume the ammonium functional groups. However, water uptake and hydroxide conductivity may notably decrease. This reduction in hydroxide conductivity may lead to the deterioration of AEMWE performance by increasing the cell's ohmic resistance. Simultaneously, AEMs may experience decreased elongation and increased elastic modulus, rendering them brittle and potentially leading to premature cell failure. The mitigation strategy of the undesired cross-linking reaction depends on their nature. When degradation byproducts participate in cross-linking reactions, it becomes crucial to prepare alkaline-stable AEMs. Increasing quaternization yield is important to reduce the number of unreacted halide groups in the polymers that can lead to cross-linking phenomena. A high quaternization yield can be achieved through homogeneous amination reactions and potentially by using a non-aqueous reaction medium.[219] Additionally, the removal of unsaturated double bonds from the polymer chain is critical in preventing undesired cross-linking.

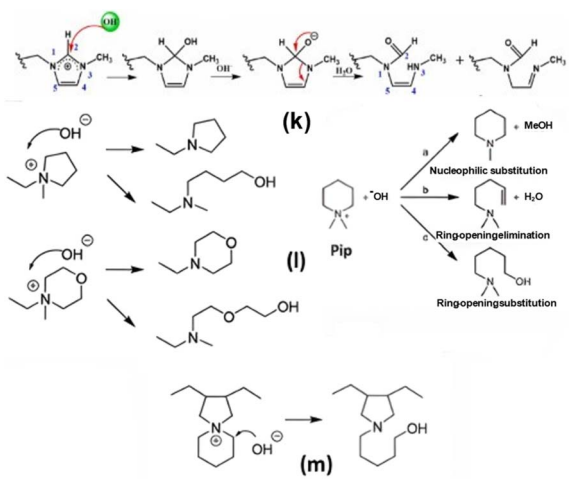

Fig. 7 Ring opening of cyclic ammonium ions: (a) ring opening of imidazolium,[202], (b) S_N2 and ring opening of piperidinium, pyrrolidinium and morpholinium,[203] and (c) ring opening of *N*-spirocyclic ammonium ions.[204] Adapted from ref. 205 (with permission from Elsevier) and ref. 194 (with permission from the Royal Society of Chemistry).

5.3.1.1.4 Membrane degradation via radicals. The migration of oxygen from the anode to the cathode compartment through the anion exchange membrane can trigger the two-electron oxygen reduction reaction, leading to the formation of hydrogen

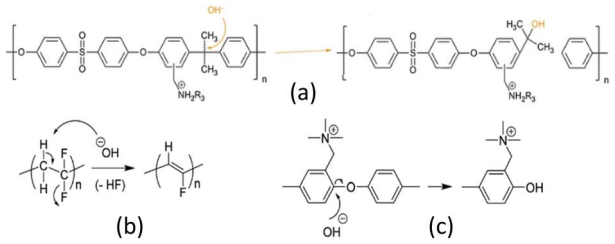

Fig. 8 Degradation pathways of the polymer backbone: (a) quaternary carbon hydrolysis, (b) dehydrofluorination, (c) aril–ether bond cleavage. Adapted from Hagesteijn *et al.*[125] (with permission from Springer Nature) and Mustain *et al.*[194] (with permission from the Royal Society of Chemistry).

peroxide radicals.[220] Additionally, hydroxyl (HO•) and hydroperoxyl (HOO•) radicals may arise from intermediates in the oxygen evolution reaction[221,222] or through cation-site catalyzed reduction of dioxygen[195,223] (Fig. 10). The detection of hydrogen peroxide in AEMWE cells suggests the likelihood of radical-induced hydrolysis of polymer electrolytes.[224,225] For evaluating resistance to radical-induced degradation, Fenton's reagent commonly serves as an *ex situ* accelerated degradation test, generating oxygen-containing free radicals in solution.[226]

Ayers *et al.* demonstrated the decline in mechanical properties of quaternized poly(arylene ether) AEMs after exposure to Fenton's test for up to 5 hours.[227] Post-Fenton's test, optical microscopy revealed surface cracking and potential dissolution of the AEMs. The predominant degradation process in polyaromatics involves the removal of OCH_3 from the methoxy-substituted compound, particularly relevant to aryl ether-containing polymers such as polysulfones and polyether ketones, causing bond breakage within the C–O–C connections.[228]

Some possible radical degradation pathways of AEMs are reported in Fig. 11. Due to its electrophilic nature, the HO• radical selectively attacks the aromatic ring near the aryl ether bond, forming phenols under high pH conditions (Fig. 11a).[228] Free radicals target the susceptible carbon (*para* position for the trimethyl ammonium hydroxide group of vinyl benzyl chloride grafts), leading to degradation of the polymer backbone in quaternized polystyrenes.[229–231] Cation degradation *via* radical attack on benzyl triethyl ammonium is also depicted in Fig. 11d.[232] In this mechanism, hydroxide ions attack the quaternary ammonium groups of the AEMs, generating ylides and water molecules through proton abstraction from the α-carbon. Subsequently, oxygen molecules in the alkaline solution capture the ylide electron, producing superoxide anion radicals and quaternary ammonium radicals, respectively. The quaternary ammonium radicals then degrade into ethylene and tertiary amine.

Notably, an increase in IEC is associated with an increase in oxidative degradation.[233] This occurrence can be ascribed to an augmented swelling ratio and water uptake, which enhance mass transport of Reactive Oxygen Species (ROS) within water channels. This improved transport, in turn, promotes the attack on vulnerable sites. Moreover, the negative impact on the stability of the AEM backbone may arise either from the

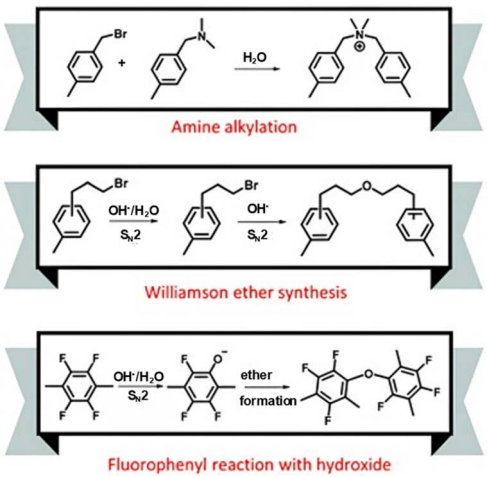

Fig. 9 Cross-linking pathways of AEMs in an alkaline environment. Adapted from Li *et al.*[163] with permission from the Royal Society of Chemistry.

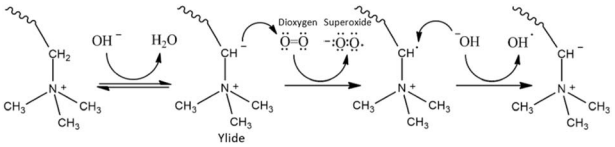

Fig. 10 Mechanism of superoxide and hydroxyl radical formation in AEMs through cation-site catalyzed reduction of dioxygen, as proposed by Parrondo *et al.*[223]

introduction of a positive headgroup, or the headgroup itself may play a catalytic or mediator role in accelerating ROS attacks on susceptible sites within the AEM. In a recent study, Maxwell *et al.*[234] used *operando* Raman spectroscopy to monitor non-PGM (Ni–Fe-based) AEMWEs during active operation. The goal was to track real-time chemical and structural changes in the electrodes and membrane (PiperION®) under electrolysis conditions. Raman analysis revealed that during oxygen evolution, new spectral bands appeared corresponding to oxygenated intermediates, indicative of reactive oxygen species (ROS) formation.

These ROS, including hydroxyl (•OH) and superoxide ($O_2^{\bullet-}$) radicals, were found to attack the ionomer and polymer membrane, leading to loss of quaternary ammonium groups and reduction in ion exchange capacity. Over extended operation, the Raman spectra showed degradation products, confirming chemical oxidation of the polymer backbone.

Practically, this work demonstrates that ROS formation in non-PGM systems can be severe and stabilizing the catalyst–ionomer interface is critical. Strategies proposed include using radical-scavenging additives, ionomers with higher oxidative resistance, and catalyst coatings that suppress peroxide and radical generation.

5.3.1.2 Mechanical membrane degradation. To induce a differential pressure during the operation of AEMWEs, both the non-porous AEM and the porous transport layer must offer robust mechanical support to withstand the pressure

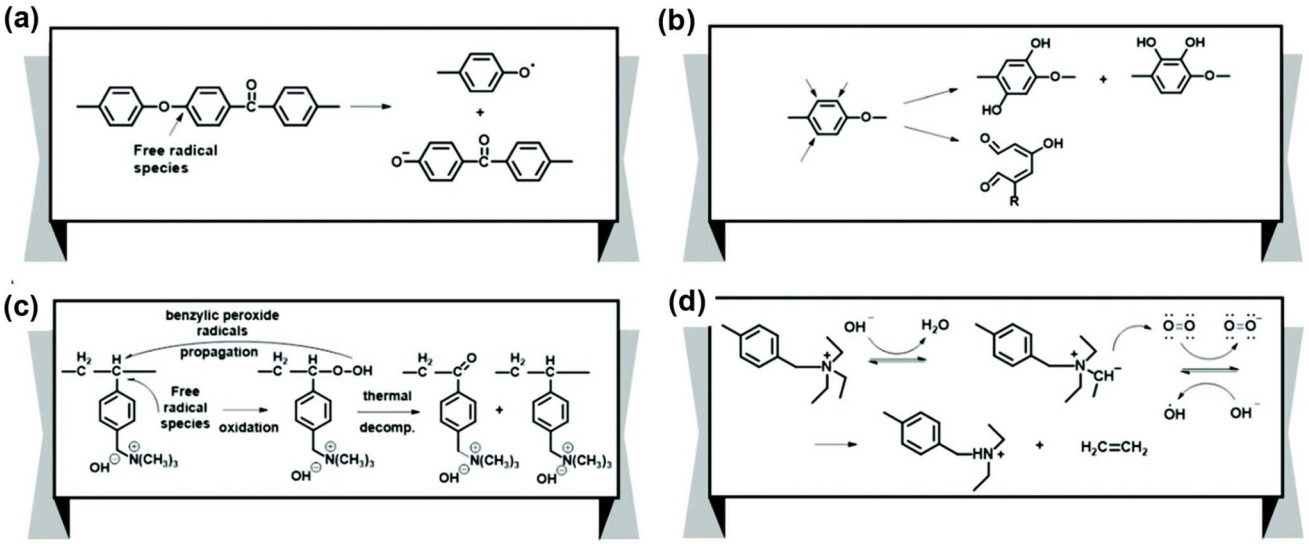

Fig. 11 Radical degradation pathways of AEMs: radicals attack both the polymer backbone and the functional groups. (a) Aryl ether polymer backbone degradation. (b) Phenyl group degradation by formation of phenolates. (c) Polymer backbone degradation of quaternized polystyrene. (d) Cationic group degradation. Adapted from Li *et al.*[163] with permission from the Royal Society of Chemistry.

disparity.[235] The maintenance of structural integrity in fully hydrated AEMs is crucial for their mechanical properties. In PEMWEs, relatively thick (125–180 μm) perfluorosulfonic acid (PFSA) membranes are commonly employed. While thicker membranes lead to higher membrane resistance, they offer advantages such as reduced gas crossover and improved mechanical robustness.[236] In contrast, AEMWEs predominantly utilize hydrocarbon AEMs due to the chemical instability of quaternized perfluorinated polymers under high pH conditions.[237] Hydrocarbon AEMs, with lower gas permeability, enable the use of thinner membranes, thereby enhancing hydrogen production efficiency.

The durability of AEMWEs is closely tied to the mechanical properties of AEMs, and their degradation often results in catastrophic performance loss.[238,239] This is frequently accompanied by an increase in high-frequency resistance (HFR), indicating potential interfacial failure between the AEM and the electrode. Predicting the time for this type of failure is challenging due to the involvement of various factors.

Post-mortem analysis reveals that mechanical failure in AEMs tends to occur at the edges of the MEA's active area, where mechanical stress is maximized.[240] For instance, a study by Wang *et al.*[241] demonstrated different cell failures using Low-Density Polyethylene (LDPE) and High-Density Polyethylene (HDPE) AEMs, which share similar IEC, thickness, water uptake, and conductivity, but differ significantly in mechanical properties. The HDPE-based AEM exhibits a stress at break of 35 MPa with an elongation at break of 283%, while the LDPE-based AEM has a stress at break of 23 MPa with an elongation at break of 35%. Tests conducted in AEMFCs reveal that the HDPE-based MEA has a lifetime exceeding 440 hours at 600 mA cm^{-2} and 70 °C under H_2/CO_2-free air conditions, whereas the LDPE-based MEA ceased testing at approximately 100 hours due to rapid mechanical cell degradation.

Mechanical degradation leads to premature failure, characterized by perforations, cracks, tears, or pinholes, which may result from inherent membrane defects or improper MEA fabrication processes. Local areas corresponding to the interface between lands and channels in the flow field or sealing edges in a cell, experiencing excessive or non-uniform mechanical stresses, are particularly susceptible to small perforations or tears. The constrained membrane in an assembled cell undergoes in-plane tension during shrinkage under low RH and in-plane compression during swelling under wet conditions. The migration and accumulation of catalysts into the membrane also negatively affect membrane conductivity and mechanical strength, significantly reducing ductility. A physical breach of the membrane due to local pinholes and perforations can result in the crossover of product gases into their respective reverse electrodes. The results from Huang *et al.*[242] suggest that the mechanical failure of the membrane initiates as a random, local imperfection that propagates to catastrophic failure.

In general, mechanical degradation problems increase as the thickness of the AEM decreases. A low membrane thickness leads to a lower electrolysis voltage caused by reduced ohmic resistance.[24] This was shown by Vidales and *et al.*[23] who used AEM thicknesses of 25, 50, and 130 μm, which resulted in an increase of the total applied voltage with increasing AEM thickness. The positive effect of low ion transport resistance and the negative effect of poor mechanical properties will need to be balanced (for example, according to the EU targets in Table 6) to result in an optimal AEM thickness.[24]

5.3.1.3 Thermal degradation. The optimal operating temperature for AEMWEs typically falls within the range of 40–80 °C to enhance conductivity and kinetics.[23] However, it introduces challenges related to durability, primarily due to the increased susceptibility to hydroxide ion (OH^-) attack. Additionally, the AEM itself may exhibit instability at elevated

temperatures, potentially undergoing glass transition or melting.

The occurrence of high-temperature spots becomes a concern if the membrane experiences breakage due to local pinholes and perforations. In such cases, there is a risk of H_2 and O_2 crossover, leading to the highly exothermic direct combustion of the oxidant and reductant on the catalyst surface, generating local hotspots. This sets off a destructive cycle wherein gas crossover and pinhole production mutually reinforce each other, inevitably accelerating the degradation of both the membrane and the entire cell.

5.3.2 Catalyst degradation. The catalyst selection for AEMWEs is greatly broadened by operation in high pH environments. In general, the intrinsic stability of HER catalysts is of less concern due to the lower cathode potential.

The most important HER catalyst degradation mechanism consists of the detachment, migration, and agglomeration of carbon supported HER catalyst nanoparticles. This degradation results from weak catalyst-supporting material interactions under alkaline conditions[243] and is accelerated by hydrogen bubble formation. Under low current density operation, hydrogen bubbles at the interface between the catalyst nanoparticles and the carbon support are not formed.[244] As the current density of the electrolyzer increases, hydrogen bubbles overcome the critical formation size (4 nm) occurring either on top of a catalyst nanoparticle or adjacent to it. As a result, catalyst nanoparticles start to detach, migrate, and agglomerate. The detachment of catalysts is prevented by using unsupported catalysts, but the catalyst's loading and cost may increase for the sake of durability improvement.

OER catalysts, conversely, still face significant stability challenges, especially upon high current density operation. Catalyst dissolution is a well-studied degradation pathway.[245] Catalysts based on the first-row transition metals, Fe, Co, and Ni, as well as their hydroxide forms, can easily dissolve into alkaline electrolytes,[246–248] but catalysts based on noble metals may also incur dissolution, the extent of which decreases in the order: Ru > Ag > Au > Ir > Rh > Pt > Pd.[249,250] At the OER potentials, noble metal catalysts can passivate by the formation of a stable oxide layer or dissolve in the electrolyte. The dissolution of metal oxides such as IrO_2 and RuO_2 is much lower than that of their metallic counterparts.[251]

It is noteworthy that even at Open Circuit Potential (OCP), catalyst dissolution differs drastically at different pH regimes. Mayerhöfer *et al.*[19] studied the dissolution of $CuCoO_x$ under different conditions observing immediate dissolution for both Cu and Co in a neutral environment at OCP, indicating the thermodynamic instability of $CuCoO_x$ at this pH. Interestingly, the metal dissolution behaviour in alkaline media is more complex and severely impacted by the ionomer activation process. The catalyst is significantly more stable in an alkaline environment than under neutral conditions. While Co and Cu are expected to form stable oxides in alkaline environments and at high potentials, neutral conditions favour the dissolution of Cu^{2+} and Co^{2+} species.[252,253]

Catalyst dissolution may lead to thermal and mechanical problems in the membrane, affecting mechanical strength and significantly reducing ductility:[254] in fact, if gas crossover happens the highly exothermic direct combustion of the oxidant and reductant occurs on the catalyst surface and consequently generates local hot-points. A destructive cycle of increasing gas crossover and pinhole production is then established, leading to inevitable degradation of membranes and their performances. Contrary to what was observed for the PEMs, performance degradation is not only due to membrane resistivity increase but also likely due to a loss of interconnection between the catalyst particles and the ionomer.[157,248]

To overcome the issue of catalyst degradation, various effective material design strategies have been developed such as doping[255–257] or surface-structure modification[258–260] of the catalyst and the formation of protective layers on the catalyst surface.[261–263]

6 Membrane degradation mitigation strategies

6.1 Chemical degradations

6.1.1 Alkaline degradation of cationic groups. To mitigate the degradation of cationic groups, various strategies have been employed. Three key approaches include:

1. *Synthesize β-hydrogen-absent cations*: by designing cations that lack β-hydrogens, which are prone to degradation, it is possible to enhance the alkaline stability of the cationic groups.

2. *Convert to coplanar arrangement and delocalize positive charges*: resonance design, such as guanidinium, imidazolium, and phosphonium, involves converting cations to a coplanar arrangement and delocalizing positive charges. This strategy aims to distribute positive charges over a broader molecular structure, reducing vulnerability to alkali attack.[8]

3. *Use cations with high steric hindrance*: in recent years, cations with high steric resistance, particularly those with cyclic or spirocyclic structures such as piperidinium and 6-azoniaspiro[5.5]undecane, have been introduced to exhibit exceptional alkaline stability.[8] Steric hindrance can in fact reduce the possibility of OH^- attack, minimizing degradations such as ring-opening reactions, addition and S_N2 substitution.

Several additional strategies have been explored to improve long-term stability against alkali attack:[264]

• *Introduction of spacer chains*: Tomoi *et al.*[265] inhibited S_N2 reactions by introducing a long spacer chain between the quaternary nitrogen atom and the benzene ring of the main chain. Alkylene spacers longer than propylene were found to make the cation less susceptible to OH^- attack.

• *Optimizing spacer length*: Hibbs *et al.*[266] designed poly(-phenylene) AEMs with hexamethylene-trimethylammonium, exhibiting superior stability compared to benzyl-trimethylammonium-containing membranes (5% *vs.* 33% conductivity loss after immersion in 4 M KOH at 90 °C for 14 days). Longer spacers were observed to impede cation degradation to some extent, potentially by increasing the Hofmann elimination barrier.

Lin *et al.*[77] reported AEM materials with different lengths of alkyl side chains between the polymer backbone and cationic

groups. Increasing the length of flexible spacers ($n \geq 4$) enhanced alkaline stability. The IEC and anion conductivity of membranes only decreased no more than 10% after treatment by 1 M KOH solution at 60 °C for 720 h. The influence of the alkylene spacer length between the AEM's backbone and the cation's head group is indeed an important aspect which deserves further investigation. However, controversy exists regarding the optimal spacer length to avoid Hofmann elimination. According to Marino and Kreuer,[76] the spacer with chain length >4 will have a negligible effect on improving the AEMs' alkaline stability. This is because the long chain fails to provide steric strain for inhibition of the Hofmann elimination reaction. Addressing this controversy may require computational chemistry and simulation to determine the precise spacer length at which the energy for hydroxide attack is highest.

In addition to the steric strain effect,[76] the influence of long spacers on enhancing microphase separation[267–269] should also be considered. Microphase separation may alter the hydration state of cations, influencing their interaction with hydroxide.

Fig. 12 illustrates the alkaline stability of commonly used cationic groups, with the half-life determined by quantitatively measuring the amount of quaternary ammonium salts before and after a given time in NaOH 6 M at a temperature of 160 °C.[76]

Fig. 13 summarizes the alkaline stability study of You *et al.*,[13] identifying the major degradation products. In this study the organic cations were subjected to 1 M or 2 M KOH/CD_3OH solution at 80 °C for 30 days with an internal standard (3-(trimethylsilyl)-1-propanesulfonic acid sodium salt, NaDSS) in sealed NMR tubes. The decomposition processes were frequently monitored by ^{1}H NMR analysis to assign the decomposition products and the dominating degradation pathways. The advantages of using methanol instead of water include good solvation of cations, accelerated degradation conditions in the presence of methoxide anions, the ability to avoid H/D exchange, and locked signals for ^{1}H NMR analysis.

Summarizing their results, it can be observed that, when possible, benzyl nucleophilic substitution predominates for ammonium cations and, alternatively, S_N2 and Hofmann elimination are both legitimate degradation pathways. For N-conjugated cations, S_N2 and Hofmann elimination are less difficult than nucleophilic addition to the iminium carbon centres, and steric hindrance is crucial in enhancing the alkaline stability of these molecules. For these types of cations, further hydrolysis and rearrangement are also frequent. Cahours–Hofmann phosphine oxidation is a specific and rapid manner for phosphonium cations to degrade, and therefore, sterically bulky substituents close to the phosphorus atom can slow this process down considerably. When utilizing electron-rich aromatic substituents on phosphorus, ether hydrolysis will likely occur under alkaline conditions. Finally, among organic cations, tetrakisaminophosphonium is proved to be one of the most stable.

In addition to the steric hindrance effect, specific stereochemistry can play a crucial role in enhancing the stability of alkaline AEMs. For example, Bauer and Strathmann[270] conducted a study on a monoquaternized 1,4-diazabicyclo[2.2.2] octane DABCO cation attached to a poly(ether sulfone) (PES) backbone. The resulting AEM exhibited remarkable resilience to OH^- attacks. Despite DABCO containing β-hydrogens, the rigid cage structure of DABCO effectively hinders the antiperiplanar conformation of the N atoms with β-hydrogen, which is a prerequisite for Hofmann elimination. This structural feature contributes to the enhanced stability of the AEM under alkaline conditions, proving that considerations may, indeed, provide valuable insights for the design and optimization of AEMs with improved alkaline stability.

6.1.2 Backbone alkaline degradation. Several strategies can be adopted to enhance alkaline stability of the polymer backbone:

- Synthesize aryl ether-free AEMs to avoid aril ether bond cleavage[72,271–273]
- Avoid electron withdrawing functional groups in the polymer backbone to mitigate the OH^- attack on the electropositive carbon.[274,275] However, one should note that even without an electron-withdrawing functional group in the polymer backbone, aryl ether-containing polymers are not as robust as aryl ether-free polymers.[271]
- Incorporate cationic functional groups far from the polymer backbone aryl ether bond[276,277]
- Use less polar polymer backbones[125]
- Control crosslinking[278–280] and the location of cationic groups to obtain optimal ion channels: to achieve an optimal location, type, and concentration of anion-conducting groups and hydrophobic side chains, through effective hydrophobic/hydrophilic region interactions, the following strategies can be pursued, depending on the polymer used: (i) linking the cationic groups to the backbone by a long aliphatic side chain,[276] (ii) synthesizing polymer main chains using multiblock co-polymers containing regions of ion-conducting groups,[281,282] (iii) using monomers with densely functionalized ion-conducting regions[283] or separately attaching the hydrophobic side chain and ion-conducting group to the polymer backbone.[284]

The optimal location, type and concentration of anion-conducting groups and hydrophobic side chains can help to achieve enhanced AEM performance through effective microphase separation. Fig. 14 shows different ion channel distributions in an AEM. The scenario depicted in Fig. 14b has been demonstrated to be the most effective. In this scenario, ion channels are created to increase anion conductivity, while the hydrophobic region protects the polymer backbone, leading to improved alkaline stability.[284]

In summary, the diverse strategies reported above highlight the importance of tailoring both the chemical structure and morphology of AEMs to achieve the desired balance between anion conductivity and stability in alkaline environments.

6.2 Mechanical degradation

Prevention of mechanical failure of MEAs is relatively easy with several mitigating strategies:

- Use edge-protect gaskets to avoid the sharp boundary between wet and dry regions of the AEM.[242,285]
- Prepare AEMs with minimal dimensional change between wet and dry states:[218,286,287] cells employing AEMs with an

Fig. 12.1 Half-life of QA compounds at $T = 160\,^{\circ}C$ in 6 M NaOH with electron-withdrawing and electron-donating substituents compared to a neutral BTM, BTE, and the TMA benchmark (entries 1–5) and DABCO- (entries 6 and 7) and piperidinium-based QAs (entries 8 and 9) with and without a benzylic group.

Entry	QA	Abbreviation[a]	Half-life [h]
1		TMA	61.9
2		MBTM	16.6
3		BTM	4.18
4		BTE	0.68
5		NBTM	0.66
6		MAABCO	13.5
7	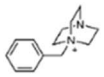	BAABCO	1.4
8		DMP	87.3
9		BMP	7.3

[a] TMA: tetramethylammonium; MBTM: 3-methoxy-benyzl trimethyl ammonium; BTM: benzyltrimethylammonium; BTE: benzyltriethylammonium; NBTM: 3-nitrobenzyltrimethylammonium; MAABCO: 1-methyl-4-aza-1-azonia-bicyclo[2.2.2]octane; BAABCO: 1-benzyl-4-aza-1-azonium-bicyclo[2.2.2]octane; DMP: *N,N*-dimethylpiperidinium; BMP: *N*-benzyl-*N*-methylpiperidinium.

Fig. 12.2 Half-lifes of BTM and various aromatic QA compounds at different temperatures in 6 M NaOH.

Entry	QA	Abbreviation[a]	Half-life [h]	T [°C]
1		BTM	4.18	160
2		PhTM	0.14	160
3		TMI	too short to measure	160
4	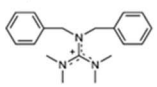	DTG	too short to measure	160
5		MOI	too short to measure	60
6	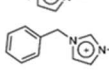	BMI	too short to measure	25
7	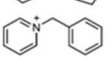	BP	too short to measure	25

[a] PhTM: phenyltrimethylammomnium; TMI: 1,2,3-trimethylimidazolium; DTG: 1,1-dibenzyl-2,2,3,3-tetramethylguaninidinium; MOI: 1-methyl-3-octylimidazolium; BMI: 1-benzyl-3-methylimidazolium; BP: *N*-benzylpyridinium.

Fig. 12.3 Half-life of alkyltrimethylammonium cations with varying side-chain length and a neopentyl-based QA at $T = 160\,^{\circ}C$ and in 6 M NaOH, ordered with respect to main-chain length.

Entry	QA	Abbreviation[a]	Half-life [h]
1		TMA	61.9
2		ETM	2.8
3		PTM	33.2
4		NTM	20.7
5		HTM	31.9
6		OTM	12.7
7		DTM	4.4
8		HexDTM	1.9

[a] ETM: ethyltrimethylammonium; PTM: propyltrimethylammonium; NTM: neopentyltrimethylammonium; HTM: hexyltrimethylammonium; OTM: octyltrimethylammonium; DTM: decyltrimethylammonium; HexDTM: hexadecyltrimethylammonium.

Fig. 12.4 Half-life of cyclic QAs and TPA (entries 1–6), the open-chain analog to ASU at 160 °C in 6 M NaOH. DABCO-based cations are compared with non-cage-like analogs (entries 7–10).

Entry	QA	Abbreviation[a]	Half-life [h]
1		ASU	110
2		DMP	87.3
3		DMPy	37.1
4		ASN	28.4
5	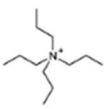	TPA	7.19
6		BMP	7.26
7		TMA	61.9
8		MAABCO	13.5
9		BTM	4.18
10	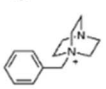	BAABCO	1.38

[a] ASU: 6-azonia-spiro[5.5]undecane; DMP: *N,N*-dimethylpiperidinium; DMPy: *N,N*-dimethylpyrrolidinium; ASN: 5-azonia-spiro[4.4]nonane; TPA: tetrapropylammonium; BMP: *N*-benzyl-*N*-methylammonium.

Fig. 12 Alkaline stability of the most common cationic groups given as half-life values. Adapted from Marino and Kreuer[76] with permission from John Wiley and Sons (License N° 5917551209635).

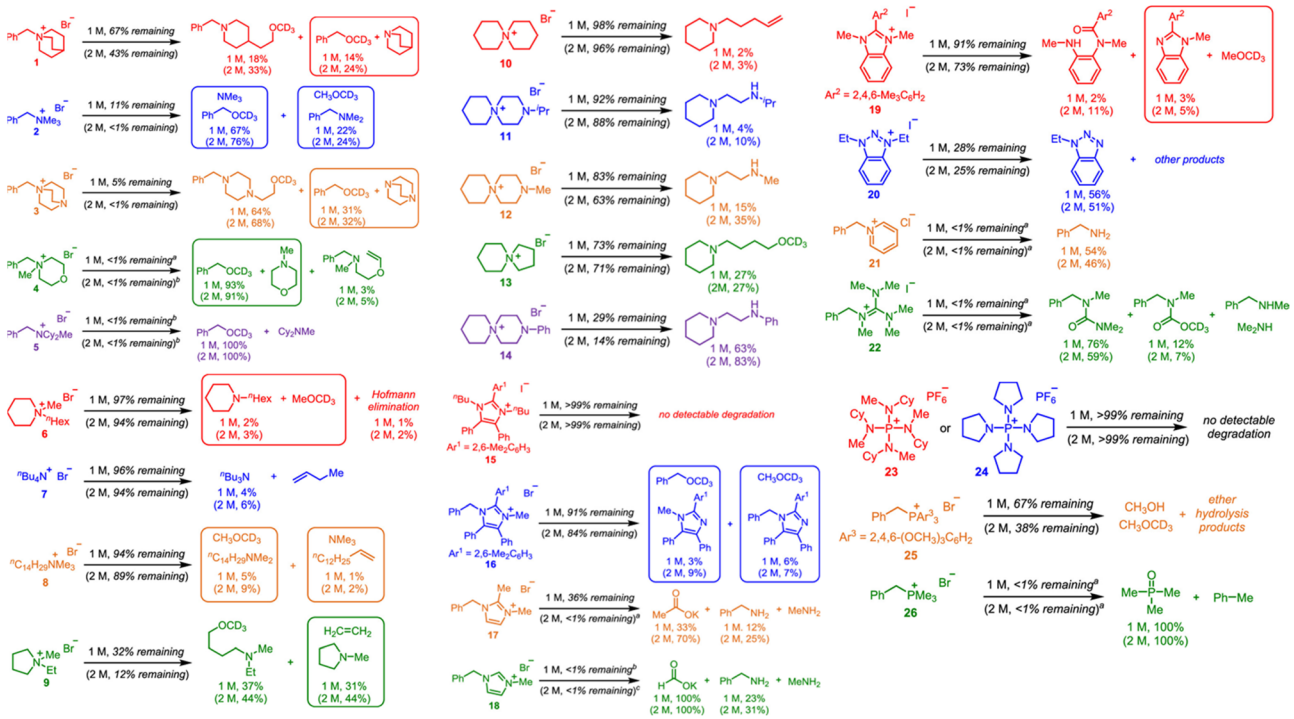

Fig. 13 Alkaline stability of the most common cationic groups and their major degradation products. Adapted with permission from You *et al.*,[13] Copyright (2020) American Chemical Society.

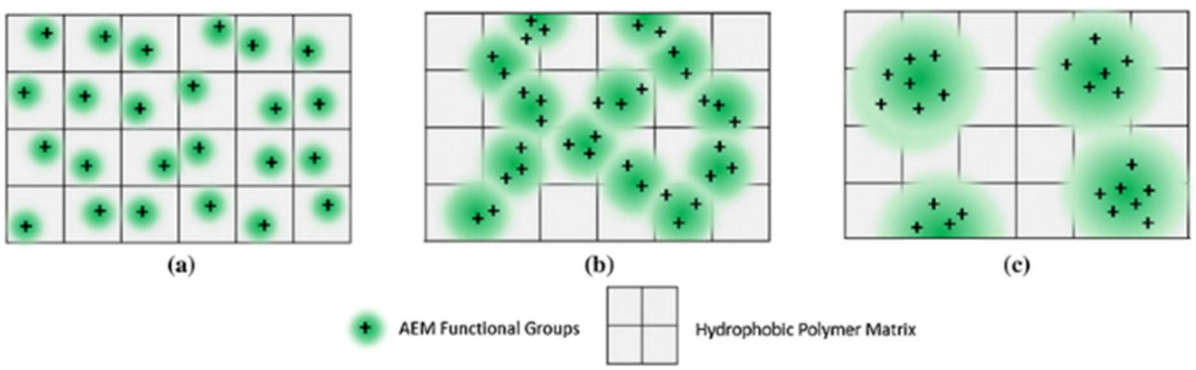

Fig. 14 Development of ion channels in AEMs. (a) Dispersed and underdeveloped ion channels, (b) interconnected ion channels conductive to the formation of "ionic highways", and (c) segregated, overdeveloped ion channels with distinct hydrophilic/hydrophobic regions. Adapted from Hagesteijn *et al.*[125] (with permission from Springer Nature).

elongation at break of >100% show stable performance without edge-failure.

• Prepare AEMs with ductile mechanical properties.[216,288,289]

• Avoid AEMs with backbone degradation: the mechanical properties of quaternized poly(arylene ether) AEMs deteriorate due to degradation reactions such as the aryl ether cleavage reaction.[206]

• Control crosslinking: Zhang *et al.*,[290] for example, designed and prepared a series of crosslinked AEMs with stable sterically protected imidazolium groups. The crosslinked AEMs have a high mechanical strength of 16.7–53.2 MPa as well as controlled water uptake and dimensional stability, especially at elevated temperature.

6.3 Addition of fillers

A way to improve the properties of polymeric membranes, including AEMs, is the development of composite materials adding 1D, 2D, and 3D inorganic fillers to enhance the thermal and mechanical properties, along with chemical stability and conductivity. Composite AEMs demonstrate superior long-term stability under alkaline conditions through synergistic effects, such as physical cross-linking (*e.g.*, acid–base interactions) or partial crystallization of the polymer near the inorganic phase.[291] Among the 1D materials, the most common are titanate and carbon nanotubes, both boosting conductivity and thermal and mechanical stability of AEMs.[292–294] The chemical and oxidative stability is also enhanced by fillers, due to the

electrostatic interactions between the filler and the polymer matrix, which can protect the cationic groups and the backbone.[292]

Among the 2D materials, the most common fillers used to enhance the AEM performance are Layered Double Hydroxides (LDHs)[295–297] and carbon-based materials such as graphene[298] and Graphene Oxide (GO).[299–301]

LDHs are inorganic lamellar ionic materials belonging to the group of anionic clays and their synthesis has a low cost. The structure of LDHs is based on $Mg(OH)_2$ brucite-type blocks where the substitution of M^{2+} with M^{3+} cations generates positively charged layers. These layers are counterbalanced by mobile anions in the interlayer, allowing for reversible insertion. The lamellae are linked by van der Waals forces. LDHs exhibit satisfactory anionic conductivity and superior stability in alkaline environments, making them effective fillers for AEMs.[296]

A very large amount of work and effort was devoted to composite AEMs containing graphene or GO. The main features of graphene are extreme mechanical resistance, great flexibility, and thermal resistance, while GO exhibits hydrophilicity and water dispersibility due to epoxy and hydroxyl groups on its basal planes, as well as carboxyl and carbonyl groups at the layer edges. These functional groups can interact with the polymer matrix *via* electrostatic and hydrogen bonding, enhancing membrane stability and diminishing OH^- activity against the electropositive polymer backbone and the conductive groups[302] of the membranes. Moreover, the sp^2 hybrid carbon structure of GO's large aromatic rings can serve as a site for scavenging oxygen free radicals generated during cell operation,[303,304] and the rich oxygen containing functional groups on its two-dimensional laminated structure can provide necessary conditions for its modification through covalent or non-covalent bonds.[305] For example, grafting conductive groups such as N-spirocyclic ammonium,[306] imidazolium,[307] and quaternary ammonium,[308,309] among others, onto the surface of GO can boost the stability and conductivity of AEMs.[310,311] Lastly, for what concerns the 3D fillers, the most studied are functionalized silica, Metal Organic Frameworks (MOFs) (that can also have 2D structures)[312–316] and metal oxide nanoparticles such zirconia, alumina and titania, which also improve AEM resistance and conductivity.[291,317–321]

7 Summary

Achieving high ionic conductivity and long-term operation of AEMs in AEMWEs is not an easy task, primarily due to the degradation of AEMs in alkaline environments, temperature, pressure and applied anode potential.

Currently, the large-scale application of AEMWEs is in fact impeded by the relatively poor durability of the commercially available AEMs: the best long-term AEMWE stability achieved is > 10 000 h in 1.0 M KOH at 1 A cm^{-2} (Motealleh *et al.*[42]) with a degradation rate of 0.7 μV h^{-1} using a Sustainion® anion exchange membrane. However, for all other AEMWEs reported here, longevity is no longer than 3000 h, highlighting the need for intensive research before the commercialization threshold of AEMWEs can be reached.

This review discussed the most used commercial AEMs, cationic functional groups and polymer backbones and then focused on their performance degradation. The relationship between design as well as operating parameters and performance of AEMs and AEMWEs has been analysed, enabling some mitigation strategies to be proposed. The optimal parameters identified are: (I) operating temperature in the 40–80 °C range and pressure within 1 to 5 MPa, to maximize performance and meet the hydrogen storage requirements, (II) feed electrolyzers with 0.1–1 M KOH solution instead of pure water, to boost the performances and minimize catalyst dissolution, (III) AEM thickness properly balanced to have low electrical resistance, high mechanical stability and low product crossover (usually 50 μm AEMs are used) and (IV) effective cell sealing to minimize CO_2 intrusion and carbonation.

Regarding AEM stability, which is the most pressing issue in AEMWEs, some guidelines can be given to obtain stable membranes. For instance, the use of a non-polar, non-fluorinated, aryl ether-free polymer backbone with functional groups far from the main chain (spacer chain length ≥ 4) is important to optimize alkaline stability, as well as the incorporation of β-hydrogen-absent cations with coplanar structures and delocalized positive charges (such as imidazolium and phosphonium) and cyclic or spirocyclic structures (such as piperidinium and 6-azonia-spiro[5.5]undecane). Also, designing interconnected ion channels through controlled crosslinking and specific location of cationic groups is also an important strategy to optimize stability and conductivity. Controlled crosslinking can be useful to mitigate radical attacks (along with the use of a radical scavenger) and enhance mechanical stability. The latter can be further improved by using an edge-protect gasket and preparing AEMs with ductile mechanical properties and minimal dimensional change between wet and dry states. Last, the addition of a filler to obtain nanocomposite AEMs can also be a viable strategy to improve mechanical, thermal and chemical stability of the membrane (and in some cases also increase conductivity). Future research on AEMWEs should focus on overcoming key scientific and engineering barriers that currently hinder large-scale commercialization. One of the most urgent priorities is the development of standardized testing and reporting protocols for membrane conductivity and durability, which would enable meaningful cross-laboratory comparison and accelerate materials optimization. In addition, enhancing the chemical, thermal and mechanical stability of AEMs remains a fundamental challenge, as degradation of both the cationic head groups and polymer backbone continues to limit operational lifetimes. Moreover, the scalable synthesis of cost-effective and environmentally friendly ionomers and membrane materials will be crucial for achieving sustainable and economically viable hydrogen production. Collectively, addressing these challenges will be essential to develop next-generation AEMWEs for green hydrogen production.

Conflicts of interest

There are no conflicts to declare.

Abbreviations

AEMWE	Anion Exchange Membrane Water Electrolyzer
PEMWE	Proton Exchange Membrane Water Electrolyzer
AEM	Anion Exchange Membrane
AEMFC	Anion Exchange Membrane Fuel Cell
PEM	Proton Exchange Membrane
PGM	Platinum Group Metal
PTLs	Porous Transport Layers
HER	Hydrogen Evolution Reaction
OER	Oxygen Evolution Reaction
QA	Quaternary Ammonium
IEC	Ion Exchange Capacity
W.U.	Water Uptake
S.R.	Swelling Ratio
EIS	Electrochemical Impedance Spectroscopy
NMR	Nuclear Magnetic Resonance
ASR	Area-Specific Resistance
LSV	Linear Sweep Voltammetry
MEA	Membrane Electrode Assembly
HFR	High-Frequency Resistance
LDPE	Low-Density Polyethylene
HDPE	High-Density Polyethylene
OCP	Open Circuit Potential
LDHs	Layered Double Hydroxides
GO	Graphene Oxide

Data availability

No primary research results, software or code have been included and no new data were generated or analysed as part of this review.

Acknowledgements

Elettrochimica ed Energia A.P.S. and Mrs Sonia Cirinnà are gratefully acknowledged for supporting the manuscript preparation.

References

1 E. S. Hanley, J. P. Deane and B. P. Ó. Gallachóir, *Renew. Sustain. Energy Rev.*, 2018, **82**, 3027–3045.
2 M. Hren, M. Božič, D. Fakin, K. S. Kleinschek and S. Gorgieva, *Sustain. Energy Fuels*, 2021, **5**, 604–637.
3 M. M. Hossen, M. S. Hasan, M. R. I. Sardar, J. bin Haider, Mottakin, K. Tammeveski and P. Atanassov, *Appl. Catal., B*, 2023, **325**, 121733.
4 H. A. Miller, K. Bouzek, J. Hnat, S. Loos, C. I. Bernäcker, T. Weißgärber, L. Röntzsch and J. Meier-Haack, *Sustain. Energy Fuels*, 2020, **4**, 2114–2133.
5 S. Y. Kang, J. E. Park, G. Y. Jang, O.-H. Kim, O. J. Kwon, Y.-H. Cho and Y.-E. Sung, *Int. J. Hydrogen Energy*, 2022, **47**, 9115–9126.
6 A. Khataee, A. Shirole, P. Jannasch, A. Krüger and A. Cornell, *J. Mater. Chem. A*, 2022, **10**, 16061–16070.
7 H. Wang, Y. Tong, K. Li and P. Chen, *J. Colloid Interface Sci.*, 2022, **628**, 306–314.
8 B. Yang and Z. Cunman, *Chem. Eng. J.*, 2023, **457**, 141094.
9 X. Chen, Y. Zhan, J. Tang, X. Yang, A. Sun, B. Lin, F. Zhu, H. Jia and X. Lei, *J. Environ. Chem. Eng.*, 2023, **11**, 110749.
10 L. J. Titheridge and A. T. Marshall, *Int. J. Hydrogen Energy*, 2024, **49**, 518–532.
11 J. Han, W. Song, X. Cheng, Q. Cheng, Y. Zhang, C. Liu, X. Zhou, Z. Ren, M. Hu, T. Ning, L. Xiao and L. Zhuang, *ChemSusChem*, 2021, **14**, 5021–5031.
12 Z. Tao, C. Wang, X. Zhao, J. Li and Q. Ren, *Mater. Chem. Front.*, 2021, **5**, 6904–6912.
13 W. You, K. M. Hugar, R. C. Selhorst, M. Treichel, C. R. Peltier, K. J. T. Noonan and G. W. Coates, *J. Org. Chem.*, 2021, **86**, 254–263.
14 N. Chen, S. Y. Paek, J. Y. Lee, J. H. Park, S. Y. Lee and Y. M. Lee, *Energy Environ. Sci.*, 2021, **14**, 6338–6348.
15 J. Xiao, A. M. Oliveira, L. Wang, Y. Zhao, T. Wang, J. Wang, B. P. Setzler and Y. Yan, *ACS Catal.*, 2021, **11**, 264–270.
16 M. S. Cha, J. E. Park, S. Kim, S.-H. Han, S.-H. Shin, S. H. Yang, T.-H. Kim, D. M. Yu, S. So, Y. T. Hong, S. J. Yoon, S.-G. Oh, S. Y. Kang, O.-H. Kim, H. S. Park, B. Bae, Y.-E. Sung, Y.-H. Cho and J. Y. Lee, *Energy Environ. Sci.*, 2020, **13**, 3633–3645.
17 Y. Ma, L. Li, X. You, H. Lin, G. Yi, X. Su, A. Zhu, Q. Liu and Q. Zhang, *Chem. Eng. J.*, 2024, **480**, 148225.
18 J. Hyun Oh, G. Ho Han, J. Kim, J. Eun Lee, H. Kim, S. Kyung Kang, H. Kim, S. Wooh, P. Soo Lee, H. Won Jang, S. Young Kim and S. Hyun Ahn, *Chem. Eng. J.*, 2023, **460**, 141727.
19 B. Mayerhöfer, F. D. Speck, M. Hegelheimer, M. Bierling, D. Abbas, D. McLaughlin, S. Cherevko, S. Thiele and R. Peach, *Int. J. Hydrogen Energy*, 2022, **47**, 4304–4314.
20 Q. Xu, L. Zhang, J. Zhang, J. Wang, Y. Hu, H. Jiang and C. Li, *EnergyChem*, 2022, **4**, 100087.
21 S. Y. Kang, J. E. Park, G. Y. Jang, O. H. Kim, O. J. Kwon, Y. H. Cho and Y. E. Sung, *Int. J. Hydrogen Energy*, 2022, **47**, 9115–9126.
22 A. Lim, M. K. Cho, S. Y. Lee, H.-J. Kim, S. J. Yoo, Y.-E. Sung, J. H. Jang and H. S. Park, *J. Electrochem. Sci. Technol.*, 2017, **8**, 265–273.
23 A. Gomez Vidales, N. C. Millan and C. Bock, *Chem. Eng. Res. Des.*, 2023, **194**, 636–648.
24 L. Zeng and T. S. Zhao, *Nano Energy*, 2015, **11**, 110–118.
25 Y. Leng, G. Chen, A. J. Mendoza, T. B. Tighe, M. A. Hickner and C.-Y. Wang, *J. Am. Chem. Soc.*, 2012, **134**, 9054–9057.
26 S. Jeong, J. Lee, S. Woo, J. Seo and B. Min, *Energies*, 2015, **8**, 7084–7099.
27 M. Faraj, M. Boccia, H. Miller, F. Martini, S. Borsacchi, M. Geppi and A. Pucci, *Int. J. Hydrogen Energy*, 2012, **37**, 14992–15002.
28 W. Ng, W. Wong, N. Rosli and K. Loh, *Separations*, 2023, **10**, 424.
29 A. H. Faqeeh and M. D. Symes, *Electrochim. Acta*, 2023, **444**, 142030.
30 A. Caprì, I. Gatto, C. Lo Vecchio, S. Trocino, A. Carbone and V. Baglio, *ChemElectroChem*, 2023, **10**(1), DOI: 10.1002/celc.202201056.
31 I. Gatto, A. Caprì, C. Lo Vecchio, S. Zignani, A. Patti and V. Baglio, *Int. J. Hydrogen Energy*, 2023, **48**, 11914–11921.

32 L. Wan, Z. Xu and B. Wang, *Chem. Eng. J.*, 2021, **426**, 131340.
33 A. Carbone, S. C. Zignani, I. Gatto, S. Trocino and A. S. Aricò, *Int. J. Hydrogen Energy*, 2020, **45**, 9285–9292.
34 S. Patra, B. Soman, T. Vineesh, N. Shyaga and T. N. Narayanan, *Mater. Chem. Front.*, 2020, **4**, 567–573.
35 D. D. Tham and D. Kim, *J. Membr. Sci.*, 2019, **581**, 139–149.
36 M. K. Cho, H.-Y. Park, H. J. Lee, H.-J. Kim, A. Lim, D. Henkensmeier, S. J. Yoo, J. Y. Kim, S. Y. Lee, H. S. Park and J. H. Jang, *J. Power Sources*, 2018, **382**, 22–29.
37 S. Ruck, A. Körner, A. Hutzler, M. Bierling, J. Gonzalez, W. Qu, C. Bock, S. Thiele, R. Peach and C. V Pham, *J. Phys.: Energy*, 2022, **4**, 044007.
38 L. Xia, W. Jiang, H. Hartmann, J. Mayer, W. Lehnert and M. Shviro, *ACS Appl. Mater. Interfaces*, 2022, **14**, 19397–19408.
39 W. Guo, J. Kim, H. Kim, S. Hong, H. Kim, S. Y. Kim and S. H. Ahn, *Mater. Today Chem.*, 2022, **24**, 100994.
40 E. López-Fernández, C. Gómez-Sacedón, J. Gil-Rostra, J. P. Espinós, J. J. Brey, A. R. González-Elipe, A. de Lucas-Consuegra and F. Yubero, *Renew. Energy*, 2022, **197**, 1183–1191.
41 N. Chen, S. Y. Paek, J. Y. Lee, J. H. Park, S. Y. Lee and Y. M. Lee, *Energy Environ. Sci.*, 2021, **14**, 6338–6348.
42 B. Motealleh, Z. Liu, R. I. Masel, J. P. Sculley, Z. Richard Ni and L. Meroueh, *Int. J. Hydrogen Energy*, 2021, **46**, 3379–3386.
43 W. Guo, J. Kim, H. Kim and S. H. Ahn, *Int. J. Hydrogen Energy*, 2021, **46**, 19789–19801.
44 Y. S. Park, J. Jeong, Y. Noh, M. J. Jang, J. Lee, K. H. Lee, D. C. Lim, M. H. Seo, W. B. Kim, J. Yang and S. M. Choi, *Appl. Catal., B*, 2021, **292**, 120170.
45 N. U. Hassan, E. Motyka, J. Kweder, P. Ganesan, B. Brechin, B. Zulevi, H. R. Colón-Mercado, P. A. Kohl and W. E. Mustain, *J. Power Sources*, 2023, **555**, 232371.
46 IRENA (2020), *Green Hydrogen Cost Reduction: Scaling up Electrolysers to Meet the 1.50C Climate Goal*, International Renewable Energy Agency, Abu Dhabi.
47 EERA European Energy Research Alliance Joint Research Programme on Fuel Cells and Hydrogen technologies (JP FCH) Implementation Plan 2018–2030.
48 H. -W. Zhang, D. -Z. Chen, Y. Xianze and S. -B. Yin, *Fuel Cells*, 2015, **15**, 761–780.
49 W. Lu, Z. Yang, H. Huang, F. Wei, W. Li, Y. Yu, Y. Gao, Y. Zhou and G. Zhang, *Ind. Eng. Chem. Res.*, 2020, **59**, 21077–21087.
50 D. Li, E. J. Park, W. Zhu, Q. Shi, Y. Zhou, H. Tian, Y. Lin, A. Serov, B. Zulevi, E. D. Baca, C. Fujimoto, H. T. Chung and Y. S. Kim, *Nat. Energy*, 2020, **5**, 378–385.
51 S. K. Tuli, A. L. Roy, R. A. Elgammal, T. A. Zawodzinski and T. Fujiwara, *Polym. Int.*, 2018, **67**, 1302–1312.
52 T. Zhou, J. Zhang, J. Jingfu, G. Jiang, J. Zhang and J. Qiao, *Synth. Met.*, 2013, **167**, 43–50.
53 T. Zhou, J. Zhang, J. Qiao, L. Liu, G. Jiang, J. Zhang and Y. Liu, *J. Power Sources*, 2013, **227**, 291–299.
54 P. Y. Xu, C. H. Zhao and Q. L. Liu, *J. Appl. Polym. Sci.*, 2013, **130**, 1172–1178.
55 J. Zhou, J. Guo, D. Chu and R. Chen, *J. Power Sources*, 2012, **219**, 272–279.
56 Q. H. Zeng, Q. L. Liu, I. Broadwell, A. M. Zhu, Y. Xiong and X. P. Tu, *J. Membr. Sci.*, 2010, **349**, 237–243.
57 J. Hong, M. Park, S. Hong and B. Kim, *J. Appl. Polym. Sci.*, 2009, **112**, 830–835.
58 J. Hong and S. Hong, *J. Appl. Polym. Sci.*, 2010, **115**, 2296–2301.
59 X. Yan, S. Gu, G. He, X. Wu and J. Benziger, *J. Power Sources*, 2014, **250**, 90–97.
60 J. Han, H. Peng, J. Pan, L. Wei, G. Li, C. Chen, L. Xiao, J. Lu and L. Zhuang, *ACS Appl. Mater. Interfaces*, 2013, **5**, 13405–13411.
61 X. Yan, G. He, S. Gu, X. Wu, L. Du and H. Zhang, *J. Membr. Sci.*, 2011, **375**, 204–211.
62 L. Zeng and T. S. Zhao, *Electrochem. Commun.*, 2013, **34**, 278–281.
63 J. Yan, H. D. Moore, M. R. Hibbs and M. A. Hickner, *J. Polym. Sci., Part B: Polym. Phys.*, 2013, **51**, 1790–1798.
64 C. Simari, M. H. Ur Rehman, A. Caprì, I. Gatto, V. Baglio and I. Nicotera, *Mater. Today Sustain.*, 2023, **21**, 100297.
65 S. S. Koilpillai and S. Dharmalingam, *Int. J. Energy Res.*, 2015, **39**, 317–325.
66 S. S. He and C. W. Frank, *J. Mater. Chem. A*, 2014, **2**, 16489–16497.
67 G. Wang, Y. Weng, J. Zhao, R. Chen and D. Xie, *J. Appl. Polym. Sci.*, 2009, **112**, 721–727.
68 G. Wang, Y. Weng, J. Zhao, D. Chu, D. Xie and R. Chen, *Polym. Adv. Technol.*, 2010, **21**, 554–560.
69 K. H. Gopi, S. G. Peera, S. D. Bhat, P. Sridhar and S. Pitchumani, *Int. J. Hydrogen Energy*, 2014, **39**, 2659–2668.
70 N. Li, L. Wang and M. Hickner, *Chem. Commun.*, 2014, **50**, 4092.
71 A. Katzfuß, S. Poynton, J. Varcoe, V. Gogel, U. Storr and J. Kerres, *J. Membr. Sci.*, 2014, **465**, 129–137.
72 W.-H. Lee, E. J. Park, J. Han, D. W. Shin, Y. S. Kim and C. Bae, *ACS Macro Lett.*, 2017, **6**, 566–570.
73 X. Wang, C. Lin, Y. Gao and R. G. H. Lammertink, *J. Membr. Sci.*, 2021, **635**, 119525.
74 Y. Wang, D. Zhang, X. Liang, M. A. Shehzad, X. Xiao, Y. Zhu, X. Ge, J. Zhang, Z. Ge, L. Wu and T. Xu, *J. Membr. Sci.*, 2020, **595**, 117483.
75 Y. Zhang, W. Chen, T. Li, X. Yan, F. Zhang, X. Wang, X. Wu, B. Pang and G. He, *J. Membr. Sci.*, 2020, **613**, 118507.
76 M. G. Marino and K. D. Kreuer, *ChemSusChem*, 2015, **8**, 513–523.
77 C. X. Lin, X. L. Huang, D. Guo, Q. G. Zhang, A. M. Zhu, M. L. Ye and Q. L. Liu, *J. Mater. Chem. A*, 2016, **4**, 13938–13948.
78 N. J. Robertson, H. A. Kostalik, T. J. Clark, P. F. Mutolo, H. D. Abruña and G. W. Coates, *J. Am. Chem. Soc.*, 2010, **132**, 3400–3404.
79 W. Liu, L. Liu, J. Liao, L. Wang and N. Li, *J. Membr. Sci.*, 2017, **536**, 133–140.
80 D. R. Dekel, M. Amar, S. Willdorf, M. Kosa, S. Dhara and C. E. Diesendruck, *Chem. Mater.*, 2017, **29**, 4425–4431.

81 J. Si, S. Lu, X. Xu, S. Peng, R. Xiu and Y. Xiang, *ChemSusChem*, 2014, **7**, 3389–3395.
82 C. Long, C. Lu, Y. Li, Z. Wang and H. Zhu, *Int. J. Hydrogen Energy*, 2020, **45**, 19778–19790.
83 U. Salma and Y. Nagao, *Polym. Degrad. Stab.*, 2020, **179**, 109299.
84 X. Gao, F. Lu, B. Dong, A. Wu, N. Sun and L. Zheng, *J. Mater. Chem. A*, 2016, **4**, 13316–13323.
85 U. Salma, D. Zhang and Y. Nagao, *ChemistrySelect*, 2020, **5**, 1255–1263.
86 D. Guo, C. X. Lin, E. N. Hu, L. Shi, F. Soyekwo, Q. G. Zhang, A. M. Zhu and Q. L. Liu, *J. Membr. Sci.*, 2017, **541**, 214–223.
87 X. Lin, X. Liang, S. D. Poynton, J. R. Varcoe, A. L. Ong, J. Ran, Y. Li, Q. Li and T. Xu, *J. Membr. Sci.*, 2013, **443**, 193–200.
88 L.-C. Jheng, C.-K. Tai, S. L.-C. Hsu, B.-Y. Lin, L. Chen, B.-C. Wang, L.-K. Chiang and W.-C. Ko, *Int. J. Hydrogen Energy*, 2017, **42**, 5315–5326.
89 C. Li, S. Zhang, S. Wang, X. Xie, C. Deng and P. Pei, *Int. J. Hydrogen Energy*, 2014, **39**, 14362–14369.
90 Y. Choi, J. Park, K. Yeon and S. Moon, *J. Membr. Sci.*, 2005, **250**, 295–304.
91 F. Gu, H. Dong, Y. Li, Z. Sun and F. Yan, *Macromolecules*, 2014, **47**, 6740–6747.
92 M. Döbbelin, I. Azcune, M. Bedu, A. Ruiz de Luzuriaga, A. Genua, V. Jovanovski, G. Cabañero and I. Odriozola, *Chem. Mater.*, 2012, **24**, 1583–1590.
93 A. N. Mondal, Y. He, L. Wu, M. I. Khan, K. Emmanuel, Md. M. Hossain, L. Ge and T. Xu, *J. Mater. Chem. A*, 2017, **5**, 1022–1027.
94 D. S. Kim, A. Labouriau, M. D. Guiver and Y. S. Kim, *Chem. Mater.*, 2011, **23**, 3795–3797.
95 T. A. Sherazi, S. Zahoor, R. Raza, A. J. Shaikh, S. A. R. Naqvi, G. Abbas, Y. Khan and S. Li, *Int. J. Hydrogen Energy*, 2015, **40**, 786–796.
96 T. Jiang, C. Wang, T. Wang, X. Wang, X. Wang, X. Li, Y. Ding and H. Wei, *J. Membr. Sci.*, 2022, **660**, 120843.
97 C. G. Morandi, R. Peach, H. M. Krieg and J. Kerres, *J. Mater. Chem. A*, 2015, **3**, 1110–1120.
98 L. Ye, L. Zhai, J. Fang, J. Liu, C. Li and R. Guan, *Solid State Ionics*, 2013, **240**, 1–9.
99 X. Wang, C. Xu, B. T. Golding, M. Sadeghi, Y. Cao and K. Scott, *Int. J. Hydrogen Energy*, 2011, **36**, 8550–8556.
100 X. Wu, W. Chen, X. Yan, G. He, J. Wang, Y. Zhang and X. Zhu, *J. Mater. Chem. A*, 2014, **2**, 12222.
101 N. Li, M. D. Guiver and W. H. Binder, *ChemSusChem*, 2013, **6**, 1376–1383.
102 L. Liu, S. He, S. Zhang, M. Zhang, M. D. Guiver and N. Li, *ACS Appl. Mater. Interfaces*, 2016, **8**, 4651–4660.
103 C. G. Arges, J. Parrondo, G. Johnson, A. Nadhan and V. Ramani, *J. Mater. Chem.*, 2012, **22**, 3733.
104 Y.-C. Cao, X. Wang, M. Mamlouk and K. Scott, *J. Mater. Chem.*, 2011, **21**, 12910.
105 C. G. Arges, L. Wang and V. Ramani, *RSC Adv.*, 2014, **4**, 61869–61876.
106 K. J. T. Noonan, K. M. Hugar, H. A. Kostalik, E. B. Lobkovsky, H. D. Abruña and G. W. Coates, *J. Am. Chem. Soc.*, 2012, **134**, 18161–18164.
107 S. Gu, J. Skovgard and Y. S. Yan, *ChemSusChem*, 2012, **5**, 843–848.
108 X. Yan, S. Gu, G. He, X. Wu, W. Zheng and X. Ruan, *J. Membr. Sci.*, 2014, **466**, 220–228.
109 S. Gu, R. Cai, T. Luo, Z. Chen, M. Sun, Y. Liu, G. He and Y. Yan, *Angew. Chem.*, 2009, **121**, 6621–6624.
110 B. Zhang, S. Gu, J. Wang, Y. Liu, A. M. Herring and Y. Yan, *RSC Adv.*, 2012, **2**, 12683.
111 Y. Zha, M. L. Disabb-Miller, Z. D. Johnson, M. A. Hickner and G. N. Tew, *J. Am. Chem. Soc.*, 2012, **134**, 4493–4496.
112 N. Chen, H. Zhu, Y. Chu, R. Li, Y. Liu and F. Wang, *Polym. Chem.*, 2017, **8**, 1381–1392.
113 M. Treichel, J. C. Gaitor, C. Birch, J. L. Vinskus and K. J. T. Noonan, *Polymer*, 2022, **249**, 124811.
114 D. R. Dekel, S. Willdorf, U. Ash, M. Amar, S. Pusara, S. Dhara, S. Srebnik and C. E. Diesendruck, *J. Power Sources*, 2018, **375**, 351–360.
115 S. Xiong, L. Ma, L. Jiang, X. Hu, G. Fu, J. Hao, H. Gao, P. Liu, L. Tan, X. Liu, Q. Wu and D. Ouyang, *Sci. Total Environ.*, 2023, **858**, 160127.
116 T. R. E. Kressman, *Nature*, 1950, **165**, 568.
117 G. Merle, M. Wessling and K. Nijmeijer, *J. Membr. Sci.*, 2011, **377**, 1–35.
118 J. Jr. Perry, *Proc., Annu. Power Sources Conf.*, 1960, **14**, 50–52.
119 J. Ahn, A. Heinzel and K. Ledjeff, *DECHEMA Monogr.*, 1990, **121**, 109.
120 D. Henkensmeier, M. Najibah, C. Harms, J. Žitka, J. Hnát and K. Bouzek, *J. Electrochem. Energy Convers. Storage*, 2021, **18**, DOI: 10.1115/1.4047963.
121 N. Ziv, W. E. Mustain and D. R. Dekel, *ChemSusChem*, 2018, **11**, 1136–1150.
122 A. Marinkas, I. Struźyńska-Piron, Y. Lee, A. Lim, H. S. Park, J. H. Jang, H.-J. Kim, J. Kim, A. Maljusch, O. Conradi and D. Henkensmeier, *Polymer*, 2018, **145**, 242–251.
123 Z. Liu, S. D. Sajjad, Y. Gao, H. Yang, J. J. Kaczur and R. I. Masel, *Int. J. Hydrogen Energy*, 2017, **42**, 29661–29665.
124 N. Ziv and D. R. Dekel, *Electrochem. Commun.*, 2018, **88**, 109–113.
125 K. F. L. Hagesteijn, S. Jiang and B. P. Ladewig, *J. Mater. Sci.*, 2018, **53**, 11131–11150.
126 J. R. Varcoe, P. Atanassov, D. R. Dekel, A. M. Herring, M. A. Hickner, P. A. Kohl, A. R. Kucernak, W. E. Mustain, K. Nijmeijer, K. Scott, T. Xu and L. Zhuang, *Energy Environ. Sci.*, 2014, **7**, 3135–3191.
127 L. Wang, Y. Liu and J. Wang, *J. Appl. Polym. Sci.*, 2019, **136**(44), DOI: 10.1002/app.48169.
128 F. Karas, J. Hnát, M. Paidar, J. Schauer and K. Bouzek, *Int. J. Hydrogen Energy*, 2014, **39**, 5054–5062.
129 O. D. Thomas, K. J. W. Y. Soo, T. J. Peckham, M. P. Kulkarni and S. Holdcroft, *J. Am. Chem. Soc.*, 2012, **134**, 10753–10756.
130 M. Khan, R. Luque, S. Akhtar, A. Shaheen, A. Mehmood, S. Idress, S. Buzdar and A. ur Rehman, *Materials*, 2016, **9**, 365.
131 L. Liu, H. Ma, M. Khan and B. S. Hsiao, *Membranes*, 2024, **14**, 85.
132 J. R. Varcoe, P. Atanassov, D. R. Dekel, A. M. Herring, M. A. Hickner, P. A. Kohl, A. R. Kucernak, W. E. Mustain,

K. Nijmeijer, K. Scott, T. Xu and L. Zhuang, *Energy Environ. Sci.*, 2014, **7**, 3135–3191.
133 D. R. Dekel, *J. Power Sources*, 2018, **375**, 158–169.
134 S. Willdorf-Cohen, A. Zhegur-Khais, J. Ponce-González, S. Bsoul-Haj, J. R. Varcoe, C. E. Diesendruck and D. R. Dekel, *ACS Appl. Energy Mater.*, 2023, **6**, 1085–1092.
135 H. Strathmann, Ion-exchange membrane separation processes, in *AmsterdamIon-exchange membrane separation processes*, 2004.
136 Y. Tanaka, S.-H. Moon, V. V. Nikonenko and T. Xu, *Int. J. Chem. Eng.*, 2012, **2012**, 1–3.
137 X. Luo, A. Wright, T. Weissbach and S. Holdcroft, *J. Power Sources*, 2018, **375**, 442–451.
138 J.-S. Park, J.-H. Choi, J.-J. Woo and S.-H. Moon, *J. Colloid Interface Sci.*, 2006, **300**, 655–662.
139 F. Müller, C. A. Ferreira, D. S. Azambuja, C. Alemán and E. Armelin, *J. Phys. Chem. B*, 2014, **118**, 1102–1112.
140 A. Zhegur-Khais, F. Kubannek, U. Krewer and D. R. Dekel, *J. Membr. Sci.*, 2020, **612**, 118461.
141 S. Jiang and B. P. Ladewig, *ACS Appl. Mater. Interfaces*, 2017, **9**, 38612–38620.
142 I. Vincent and D. Bessarabov, *Renew. Sustain. Energy Rev.*, 2018, **81**, 1690–1704.
143 Z. Li, X. He, Z. Jiang, Y. Yin, B. Zhang, G. He, Z. Tong, H. Wu and K. Jiao, *Electrochim. Acta*, 2017, **240**, 486–494.
144 R. Narducci, J.-F. Chailan, A. Fahs, L. Pasquini, M. L. Di Vona and P. Knauth, *J. Polym. Sci., Part B: Polym. Phys.*, 2016, **54**, 1180–1187.
145 Y. Wu, C. Wu, T. Xu and Y. Fu, *J. Membr. Sci.*, 2009, **329**, 236–245.
146 freeTextSearchKeyword=AEM;typeCodes=1;statusCodes=31094501,31094502;programCode=H2020;programDivisionCode=null;focusAreaCode=null;crossCuttingPriorityCode=null;callCode=Default;sortQuery=openingDate;orderBy=asc;onlyTenders=false, https://ec.europa.eu/info/funding-tenders/opportunities/portal/screen/opportunities/topic-details/fch-02-4-2019.
147 S. Ratso, I. Kruusenberg, U. Joost, R. Saar and K. Tammeveski, *Int. J. Hydrogen Energy*, 2016, **41**, 22510–22519.
148 S. Kabir, A. Zadick, P. Atanassov, L. Dubau and M. Chatenet, *Electrochem. Commun.*, 2017, **78**, 33–37.
149 H. A. Miller, F. Vizza, M. Marelli, A. Zadick, L. Dubau, M. Chatenet, S. Geiger, S. Cherevko, H. Doan, R. K. Pavlicek, S. Mukerjee and D. R. Dekel, *Nano Energy*, 2017, **33**, 293–305.
150 W. Tong, M. Forster, F. Dionigi, S. Dresp, R. Sadeghi Erami, P. Strasser, A. J. Cowan and P. Farràs, *Nat. Energy*, 2020, **5**, 367–377.
151 G. A. Lindquist, Q. Xu, S. Z. Oener and S. W. Boettcher, *Joule*, 2020, **4**, 2549–2561.
152 L. An, T. S. Zhao, Z. H. Chai, P. Tan and L. Zeng, *Int. J. Hydrogen Energy*, 2014, **39**, 19869–19876.
153 M. K. Cho, H.-Y. Park, S. Choe, S. J. Yoo, J. Y. Kim, H.-J. Kim, D. Henkensmeier, S. Y. Lee, Y.-E. Sung, H. S. Park and J. H. Jang, *J. Power Sources*, 2017, **347**, 283–290.
154 B. Han, S. M. Steen, J. Mo and F.-Y. Zhang, *Int. J. Hydrogen Energy*, 2015, **40**, 7006–7016.
155 V. Liso, G. Savoia, S. S. Araya, G. Cinti and S. K. Kær, *Energies*, 2018, **11**, 3273.
156 F. Marangio, M. Santarelli and M. Cali, *Int. J. Hydrogen Energy*, 2009, **34**, 1143–1158.
157 D. Xu, M. B. Stevens, M. R. Cosby, S. Z. Oener, A. M. Smith, L. J. Enman, K. E. Ayers, C. B. Capuano, J. N. Renner, N. Danilovic, Y. Li, H. Wang, Q. Zhang and S. W. Boettcher, *ACS Catal.*, 2019, **9**, 7–15.
158 F. Marangio, M. Santarelli and M. Cali, *Int. J. Hydrogen Energy*, 2009, **34**, 1143–1158.
159 I. V. Pushkareva, A. S. Pushkarev, S. A. Grigoriev, P. Modisha and D. G. Bessarabov, *Int. J. Hydrogen Energy*, 2020, **45**, 26070–26079.
160 M. Mandal, *ChemElectroChem*, 2021, **8**, 36–45.
161 G. A. Lindquist, S. Z. Oener, R. Krivina, A. R. Motz, A. Keane, C. Capuano, K. E. Ayers and S. W. Boettcher, *ACS Appl. Mater. Interfaces*, 2021, **13**, 51917–51924.
162 M. R. Kraglund, M. Carmo, G. Schiller, S. A. Ansar, D. Aili, E. Christensen and J. O. Jensen, *Energy Environ. Sci.*, 2019, **12**, 3313–3318.
163 D. Li, A. R. Motz, C. Bae, C. Fujimoto, G. Yang, F.-Y. Zhang, K. E. Ayers and Y. S. Kim, *Energy Environ. Sci.*, 2021, **14**, 3393–3419.
164 R. A. Krivina, G. A. Lindquist, M. C. Yang, A. K. Cook, C. H. Hendon, A. R. Motz, C. Capuano, K. E. Ayers, J. E. Hutchison and S. W. Boettcher, *ACS Appl. Mater. Interfaces*, 2022, **14**, 18261–18274.
165 X. Chu, Y. Shi, L. Liu, Y. Huang and N. Li, *J. Mater. Chem. A*, 2019, **7**, 7717–7727.
166 T. Pandiarajan, L. John Berchmans and S. Ravichandran, *RSC Adv.*, 2015, **5**, 34100–34108.
167 X. Luo, D. I. Kushner, J. Li, E. J. Park, Y. S. Kim and A. Kusoglu, *Adv. Funct. Mater.*, 2021, **31**(20), DOI: 10.1002/adfm.202008778.
168 Y. S. Kim, *ACS Appl. Polym. Mater.*, 2021, **3**, 1250–1270.
169 D. Li, I. Matanovic, A. S. Lee, E. J. Park, C. Fujimoto, H. T. Chung and Y. S. Kim, *ACS Appl. Mater. Interfaces*, 2019, **11**, 9696–9701.
170 S. Maurya, A. S. Lee, D. Li, E. J. Park, D. P. Leonard, S. Noh, C. Bae and Y. S. Kim, *J. Power Sources*, 2019, **436**, 226866.
171 D. Li, H. T. Chung, S. Maurya, I. Matanovic and Y. S. Kim, *Curr. Opin. Electrochem.*, 2018, **12**, 189–195.
172 I. Matanovic, S. Maurya, E. J. Park, J. Y. Jeon, C. Bae and Y. S. Kim, *Chem. Mater.*, 2019, **31**, 4195–4204.
173 M. S. Ide, B. Hao, M. Neurock and R. J. Davis, *ACS Catal.*, 2012, **2**, 671–683.
174 A. K. Niaz, A. Akhtar, J.-Y. Park and H.-T. Lim, *J. Power Sources*, 2021, **481**, 229093.
175 W. A. Rigdon, T. J. Omasta, C. Lewis, M. A. Hickner, J. R. Varcoe, J. N. Renner, K. E. Ayers and W. E. Mustain, *J. Electrochem. Energy Convers. Storage*, 2017, **14**(2), DOI: 10.1115/1.4033411.
176 M. Inaba, Y. Matsui, M. Saito, A. Tasaka, K. Fukuta, S. Watanabe and H. Yanagi, *Electrochemistry*, 2011, **79**, 322–325.

177 Y. Zheng, T. J. Omasta, X. Peng, L. Wang, J. R. Varcoe, B. S. Pivovar and W. E. Mustain, *Energy Environ. Sci.*, 2019, **12**, 2806–2819.
178 M. R. Gerhardt, L. M. Pant and A. Z. Weber, *J. Electrochem. Soc.*, 2019, **166**, F3180–F3192.
179 M. R. Gerhardt, L. M. Pant, H.-S. Shiau and A. Z. Weber, *ECS Trans.*, 2018, **86**, 15–24.
180 J. A. Wrubel, A. A. Peracchio, B. N. Cassenti, T. D. Myles, K. N. Grew and W. K. S. Chiu, *J. Electrochem. Soc.*, 2017, **164**, F1063–F1073.
181 J. Parrondo, C. G. Arges, M. Niedzwiecki, E. B. Anderson, K. E. Ayers and V. Ramani, *RSC Adv.*, 2014, **4**, 9875.
182 J. Li, C. Liu, J. Ge, W. Xing and J. Zhu, *Chem.–Eur. J.*, 2023, **29**(26), DOI: 10.1002/chem.202203173.
183 A. collier, H. wang, X. ziyuan, J. Zhang and D. Wilkinson, *Int. J. Hydrogen Energy*, 2006, **31**, 1838–1854.
184 M. Ramdin, O. A. Moultos, L. J. P. van den Broeke, P. Gonugunta, P. Taheri and T. J. H. Vlugt, *Ind. Eng. Chem. Res.*, 2023, **62**, 6843–6864.
185 B. Chen, P. Mardle and S. Holdcroft, *J. Power Sources*, 2022, **550**, 232134.
186 A. Martinez-Lazaro, A. Caprì, I. Gatto, J. Ledesma-García, N. Rey-Raap, A. Arenillas, F. I. Espinosa-Lagunes, V. Baglio and L. G. Arriaga, *J. Power Sources*, 2023, **556**, 232417.
187 S. Campagna Zignani, M. Lo Faro, A. Carbone, C. Italiano, S. Trocino, G. Monforte and A. S. Aricò, *Electrochim. Acta*, 2022, **413**, 140078.
188 G. Huang, M. Mandal, N. U. Hassan, K. Groenhout, A. Dobbs, W. E. Mustain and P. A. Kohl, *J. Electrochem. Soc.*, 2021, **168**, 024503.
189 S. Raiguel, W. Dehaen and K. Binnemans, *Green Chem.*, 2020, **22**, 5225–5252.
190 C. G. Arges and V. Ramani, *Proc. Natl. Acad. Sci. U. S. A.*, 2013, **110**, 2490–2495.
191 T. S. Stevens, E. M. Creighton, A. B. Gordon and M. MacNicol, *J. Chem. Soc.*, 1928, **0**, 3193–3197.
192 C. T. Womble, J. Kang, K. M. Hugar, G. W. Coates, S. Bernhard and K. J. T. Noonan, *Organometallics*, 2017, **36**, 4038–4046.
193 Z. Zakaria and S. K. Kamarudin, *Int. J. Energy Res.*, 2021, **45**, 18337–18354.
194 W. E. Mustain, M. Chatenet, M. Page and Y. S. Kim, *Energy Environ. Sci.*, 2020, **13**, 2805–2838.
195 S. Wierzbicki, J. C. Douglin, A. Kostuch, D. R. Dekel and K. Kruczała, *J. Phys. Chem. Lett.*, 2020, **11**, 7630–7636.
196 A. D. Mohanty and C. Bae, *J. Mater. Chem. A*, 2014, **2**, 17314–17320.
197 P. G. Stevens and J. H. Richmond, *J. Am. Chem. Soc.*, 1941, **63**, 3132–3136.
198 G. Ghigo, S. Cagnina, A. Maranzana and G. Tonachini, *J. Org. Chem.*, 2010, **75**, 3608–3617.
199 S. Chempath, J. M. Boncella, L. R. Pratt, N. Henson and B. S. Pivovar, *J. Phys. Chem. C*, 2010, **114**, 11977–11983.
200 A. Vöge, V. Deimede and J. K. Kallitsis, *RSC Adv.*, 2014, **4**, 45040–45049.
201 W. Li, S. Wang, X. Zhang, W. Wang, X. Xie and P. Pei, *Int. J. Hydrogen Energy*, 2014, **39**, 13710–13717.
202 B. Lee, D. Yun, J.-S. Lee, C. H. Park and T.-H. Kim, *J. Phys. Chem. C*, 2019, **123**, 13508–13518.
203 H.-S. Dang and P. Jannasch, *J. Mater. Chem. A*, 2017, **5**, 21965–21978.
204 J. S. Olsson, T. H. Pham and P. Jannasch, *Macromolecules*, 2020, **53**, 4722–4732.
205 U. Salma and N. Shalahin, *Results Mater.*, 2023, **17**, 100366.
206 R.-A. Becerra-Arciniegas, R. Narducci, G. Ercolani, S. Antonaroli, E. Sgreccia, L. Pasquini, P. Knauth and M. L. Di Vona, *Polymer*, 2019, **185**, 121931.
207 C. Fujimoto, D.-S. Kim, M. Hibbs, D. Wrobleski and Y. S. Kim, *J. Membr. Sci.*, 2012, **423–424**, 438–449.
208 S. Miyanishi and T. Yamaguchi, *Phys. Chem. Chem. Phys.*, 2016, **18**, 12009–12023.
209 A. Amel, L. Zhu, M. Hickner and Y. Ein-Eli, *J. Electrochem. Soc.*, 2014, **161**, F615–F621.
210 J. Sharma and V. Kulshrestha, in *Alkaline Anion Exchange Membranes for Fuel Cells*, Wiley, 2024, pp. 241–284.
211 Y.-K. Choe, C. Fujimoto, K.-S. Lee, L. T. Dalton, K. Ayers, N. J. Henson and Y. S. Kim, *Chem. Mater.*, 2014, **26**, 5675–5682.
212 L. Liu, X. Chu, J. Liao, Y. Huang, Y. Li, Z. Ge, M. A. Hickner and N. Li, *Energy Environ. Sci.*, 2018, **11**, 435–446.
213 Q. Ge, J. Ran, J. Miao, Z. Yang and T. Xu, *ACS Appl. Mater. Interfaces*, 2015, **7**, 28545–28553.
214 L. Zhu, T. J. Zimudzi, N. Li, J. Pan, B. Lin and M. A. Hickner, *Polym. Chem.*, 2016, **7**, 2464–2475.
215 Y. He, L. Wu, J. Pan, Y. Zhu, X. Ge, Z. Yang, J. Ran and T. Xu, *J. Membr. Sci.*, 2016, **504**, 47–54.
216 J. Y. Jeon, S. Park, J. Han, S. Maurya, A. D. Mohanty, D. Tian, N. Saikia, M. A. Hickner, C. Y. Ryu, M. E. Tuckerman, S. J. Paddison, Y. S. Kim and C. Bae, *Macromolecules*, 2019, **52**, 2139–2147.
217 S. Miyanishi and T. Yamaguchi, *Polym. Chem.*, 2020, **11**, 3812–3820.
218 Md. M. Hossain, L. Wu, X. Liang, Z. Yang, J. Hou and T. Xu, *J. Power Sources*, 2018, **390**, 234–241.
219 E. J. Park, S. Maurya, M. R. Hibbs, C. H. Fujimoto, K.-D. Kreuer and Y. S. Kim, *Macromolecules*, 2019, **52**, 5419–5428.
220 F. D. Speck, P. G. Santori, F. Jaouen and S. Cherevko, *J. Phys. Chem. C*, 2019, **123**, 25267–25277.
221 K. Juodkazis, J. Juodkazytė, R. Vilkauskaitė and V. Jasulaitienė, *J. Solid State Electrochem.*, 2008, **12**, 1469–1479.
222 S. Loos, I. Zaharieva, P. Chernev, A. Lißner and H. Dau, *ChemSusChem*, 2019, **12**, 1966–1976.
223 J. Parrondo, Z. Wang, M.-S. J. Jung and V. Ramani, *Phys. Chem. Chem. Phys.*, 2016, **18**, 19705–19712.
224 H. Kaczmarek, L. Å. Lindén and J. F. Rabek, *Polym. Degrad. Stab.*, 1995, **47**, 175–188.
225 R. Espiritu, B. T. Golding, K. Scott and M. Mamlouk, *J. Power Sources*, 2018, **375**, 373–386.
226 R. Borup, J. Meyers, B. Pivovar, Y. S. Kim, R. Mukundan, N. Garland, D. Myers, M. Wilson, F. Garzon, D. Wood,

P. Zelenay, K. More, K. Stroh, T. Zawodzinski, J. Boncella, J. E. McGrath, M. Inaba, K. Miyatake, M. Hori, K. Ota, Z. Ogumi, S. Miyata, A. Nishikata, Z. Siroma, Y. Uchimoto, K. Yasuda, K. Kimijima and N. Iwashita, *Chem. Rev.*, 2007, **107**, 3904–3951.

227 K. E. Ayers, E. B. Anderson, C. B. Capuano, M. Niedzwiecki, M. A. Hickner, C.-Y. Wang, Y. Leng and W. Zhao, *ECS Trans.*, 2013, **45**, 121–130.

228 G. Hübner and E. Roduner, *J. Mater. Chem.*, 1999, **9**, 409–418.

229 Y.-F. He, R.-M. Wang, Y.-Y. Liu, Y. Chang, Y.-P. Wang, C.-G. Xia and J.-S. Suo, *J. Mol. Catal. A: Chem.*, 2000, **159**, 109–113.

230 R. Espiritu, B. T. Golding, K. Scott and M. Mamlouk, *J. Mater. Chem. A*, 2017, **5**, 1248–1267.

231 I. Di Somma, R. Andreozzi, M. Canterino, V. Caprio and R. Sanchirico, *AIChE J.*, 2008, **54**, 1579–1584.

232 N. Ye, Y. Xu, D. Zhang, J. Yang and R. He, *Polym. Degrad. Stab.*, 2018, **153**, 298–306.

233 Z. Feng, G. Gupta and M. Mamlouk, *RSC Adv.*, 2023, **13**, 20235–20242.

234 D. S. Maxwell, I. Kendrick and S. Mukerjee, *J. Am. Chem. Soc.*, 2024, **146**, 22431–22444.

235 U. Babic, M. Suermann, F. N. Büchi, L. Gubler and T. J. Schmidt, *J. Electrochem. Soc.*, 2017, **164**, F387–F399.

236 A. Albert, A. O. Barnett, M. S. Thomassen, T. J. Schmidt and L. Gubler, *ACS Appl. Mater. Interfaces*, 2015, **7**, 22203–22212.

237 D. S. Kim, C. H. Fujimoto, M. R. Hibbs, A. Labouriau, Y.-K. Choe and Y. S. Kim, *Macromolecules*, 2013, **46**, 7826–7833.

238 C. Fujimoto, D.-S. Kim, M. Hibbs, D. Wrobleski and Y. S. Kim, *J. Membr. Sci.*, 2012, **423–424**, 438–449.

239 J. Lei, Z. Wang, Y. Zhang, M. Ju, H. Fei, S. Wang, C. Fu, X. Yuan, Q. Fu, M. U. Farid, H. Kong, A. K. An, R. Deng, F. Liu and J. Wang, *Carbon Neutrality*, 2024, **3**, 25.

240 K. H. Lee, D. H. Cho, Y. M. Kim, S. J. Moon, J. G. Seong, D. W. Shin, J.-Y. Sohn, J. F. Kim and Y. M. Lee, *Energy Environ. Sci.*, 2017, **10**, 275–285.

241 L. Wang, X. Peng, W. E. Mustain and J. R. Varcoe, *Energy Environ. Sci.*, 2019, **12**, 1575–1579.

242 X. Huang, R. Solasi, Y. Zou, M. Feshler, K. Reifsnider, D. Condit, S. Burlatsky and T. Madden, *J. Polym. Sci., Part B: Polym. Phys.*, 2006, **44**, 2346–2357.

243 Q. Wang, Y. Gao, Z. Ma, Y. Zhang, W. Ni, H. A. Younus, C. Zhang, Z. Chen and S. Zhang, *J. Energy Chem.*, 2021, **54**, 342–351.

244 P. Paciok, M. Schalenbach, M. Carmo and D. Stolten, *J. Power Sources*, 2017, **365**, 53–60.

245 H. Jin, B. Ruqia, Y. Park, H. J. Kim, H. Oh, S. Choi and K. Lee, *Adv. Energy Mater.*, 2020, **11**(4), DOI: 10.1002/aenm.202003188.

246 J. Staszak-Jirkovský, C. D. Malliakas, P. P. Lopes, N. Danilovic, S. S. Kota, K.-C. Chang, B. Genorio, D. Strmcnik, V. R. Stamenkovic, M. G. Kanatzidis and N. M. Markovic, *Nat. Mater.*, 2016, **15**, 197–203.

247 Y. Zhang, L. Gao, E. J. M. Hensen and J. P. Hofmann, *ACS Energy Lett.*, 2018, **3**, 1360–1365.

248 L. Xie and D. W. Kirk, *Electrochim. Acta*, 2020, **364**, 137091.

249 S. Cherevko, A. R. Zeradjanin, G. P. Keeley and K. J. J. Mayrhofer, *J. Electrochem. Soc.*, 2014, **161**, H822–H830.

250 M. Schalenbach, O. Kasian, M. Ledendecker, F. D. Speck, A. M. Mingers, K. J. J. Mayrhofer and S. Cherevko, *Electrocatalysis*, 2018, **9**, 153–161.

251 S. Cherevko, S. Geiger, O. Kasian, N. Kulyk, J.-P. Grote, A. Savan, B. R. Shrestha, S. Merzlikin, B. Breitbach, A. Ludwig and K. J. J. Mayrhofer, *Catal. Today*, 2016, **262**, 170–180.

252 F. D. Speck and S. Cherevko, *Electrochem. Commun.*, 2020, **115**, 106739.

253 C. Stumm, M. Bertram, M. Kastenmeier, F. D. Speck, Z. Sun, J. Rodríguez-Fernández, J. V. Lauritsen, K. J. J. Mayrhofer, S. Cherevko, O. Brummel and J. Libuda, *Adv. Funct. Mater.*, 2021, **31**(13), DOI: 10.1002/adfm.202009923.

254 J. Wu, X. Z. Yuan, J. J. Martin, H. Wang, J. Zhang, J. Shen, S. Wu and W. Merida, *J. Power Sources*, 2008, **184**, 104–119.

255 J. W. D. Ng, M. García-Melchor, M. Bajdich, P. Chakthranont, C. Kirk, A. Vojvodic and T. F. Jaramillo, *Nat. Energy*, 2016, **1**, 16053.

256 C. Guan, W. Xiao, H. Wu, X. Liu, W. Zang, H. Zhang, J. Ding, Y. P. Feng, S. J. Pennycook and J. Wang, *Nano Energy*, 2018, **48**, 73–80.

257 C. Tang, R. Zhang, W. Lu, L. He, X. Jiang, A. M. Asiri and X. Sun, *Adv. Mater.*, 2017, **29**(2), DOI: 10.1002/adma.201602441.

258 F. Yu, H. Zhou, Z. Zhu, J. Sun, R. He, J. Bao, S. Chen and Z. Ren, *ACS Catal.*, 2017, **7**, 2052–2057.

259 K. Liu, C. Zhang, Y. Sun, G. Zhang, X. Shen, F. Zou, H. Zhang, Z. Wu, E. C. Wegener, C. J. Taubert, J. T. Miller, Z. Peng and Y. Zhu, *ACS Nano*, 2018, **12**, 158–167.

260 P. Chen, K. Xu, Z. Fang, Y. Tong, J. Wu, X. Lu, X. Peng, H. Ding, C. Wu and Y. Xie, *Angew. Chem., Int. Ed.*, 2015, **54**, 14710–14714.

261 J. Mahmood, M. A. R. Anjum, S. Shin, I. Ahmad, H. Noh, S. Kim, H. Y. Jeong, J. S. Lee and J. Baek, *Adv. Mater.*, 2018, **30**(52), DOI: 10.1002/adma.201805606.

262 L. Ai, T. Tian and J. Jiang, *ACS Sustain. Chem. Eng.*, 2017, **5**, 4771–4777.

263 L. Du, L. Luo, Z. Feng, M. Engelhard, X. Xie, B. Han, J. Sun, J. Zhang, G. Yin, C. Wang, Y. Wang and Y. Shao, *Nano Energy*, 2017, **39**, 245–252.

264 J. Pan, H. Zhu, H. Cao, B. Wang, J. Zhao, Z. Sun and F. Yan, *J. Membr. Sci.*, 2021, **620**, 118794.

265 M. Tomoi, K. Yamaguchi, R. Ando, Y. Kantake, Y. Aosaki and H. Kubota, *J. Appl. Polym. Sci.*, 1997, **64**, 1161–1167.

266 M. R. Hibbs, *J. Polym. Sci., Part B: Polym. Phys.*, 2013, **51**, 1736–1742.

267 N. Li, Y. Leng, M. A. Hickner and C.-Y. Wang, *J. Am. Chem. Soc.*, 2013, **135**, 10124–10133.

268 N. Li, T. Yan, Z. Li, T. Thurn-Albrecht and W. H. Binder, *Energy Environ. Sci.*, 2012, **5**, 7888.

269 J. Ran, L. Wu, B. Wei, Y. Chen and T. Xu, *Sci. Rep.*, 2014, **4**, 6486.

270 B. Bauer, H. Strathmann and F. Effenberger, *Desalination*, 1990, **79**, 125–144.
271 E. J. Park and Y. S. Kim, *J. Mater. Chem. A*, 2018, **6**, 15456–15477.
272 T. H. Pham, J. S. Olsson and P. Jannasch, *J. Mater. Chem. A*, 2019, **7**, 15895–15906.
273 X. Wang, W. Sheng, Y. Shen, L. Liu, S. Dai and N. Li, *J. Membr. Sci.*, 2019, **587**, 117135.
274 A. Amel, S. B. Smedley, D. R. Dekel, M. A. Hickner and Y. Ein-Eli, *J. Electrochem. Soc.*, 2015, **162**, F1047–F1055.
275 C. G. Arges, L. Wang, M. Jung and V. Ramani, *J. Electrochem. Soc.*, 2015, **162**, F686–F693.
276 J. Han, Q. Liu, X. Li, J. Pan, L. Wei, Y. Wu, H. Peng, Y. Wang, G. Li, C. Chen, L. Xiao, J. Lu and L. Zhuang, *ACS Appl. Mater. Interfaces*, 2015, **7**, 2809–2816.
277 J. Pan, J. Han, L. Zhu and M. A. Hickner, *Chem. Mater.*, 2017, **29**, 5321–5330.
278 W. You, K. M. Hugar and G. W. Coates, *Macromolecules*, 2018, **51**, 3212–3218.
279 S.-B. Lee, C.-M. Min, J. Jang and J.-S. Lee, *Polymer*, 2020, **192**, 122331.
280 Q. Yang, X. L. Gao, H. Y. Wu, Y. Y. Cai, Q. G. Zhang, A. M. Zhu and Q. L. Liu, *J. Power Sources*, 2019, **436**, 226856.
281 E. A. Weiber, D. Meis and P. Jannasch, *Polym. Chem.*, 2015, **6**, 1986–1996.
282 X. Ren, S. C. Price, A. C. Jackson, N. Pomerantz and F. L. Beyer, *ACS Appl. Mater. Interfaces*, 2014, **6**, 13330–13333.
283 D. Chen and M. A. Hickner, *Macromolecules*, 2013, **46**, 9270–9278.
284 J. Pan, C. Chen, Y. Li, L. Wang, L. Tan, G. Li, X. Tang, L. Xiao, J. Lu and L. Zhuang, *Energy Environ. Sci.*, 2014, **7**, 354–360.
285 H. Ishikawa, T. Teramoto, Y. Ueyama, Y. Sugawara, Y. Sakiyama, M. Kusakabe, K. Miyatake and M. Uchida, *J. Power Sources*, 2016, **325**, 35–41.
286 L. Zhu, T. J. Zimudzi, N. Li, J. Pan, B. Lin and M. A. Hickner, *Polym. Chem.*, 2016, **7**, 2589.
287 X. Q. Wang, C. X. Lin, F. H. Liu, L. Li, Q. Yang, Q. G. Zhang, A. M. Zhu and Q. L. Liu, *J. Mater. Chem. A*, 2018, **6**, 12455–12465.
288 C. Xiao Lin, X. Qin Wang, E. Ning Hu, Q. Yang, Q. Gen Zhang, A. Mei Zhu and Q. Lin Liu, *J. Membr. Sci.*, 2017, **541**, 358–366.
289 P. Dai, Z.-H. Mo, R.-W. Xu, S. Zhang and Y.-X. Wu, *ACS Appl. Mater. Interfaces*, 2016, **8**, 20329–20341.
290 X. Zhang, Y. Cao, M. Zhang, Y. Huang, Y. Wang, L. tableLiu and N. Li, *J. Membr. Sci.*, 2020, **596**, 117700.
291 R. Narducci, E. Sgreccia, P. Knauth and M. L. Di Vona, *Polymers*, 2021, **13**, 3887.
292 T. Zhou, M. Wang, X. He and J. Qiao, *J. Materiomics*, 2019, **5**, 286–295.
293 V. Elumalai and D. Sangeetha, *J. Power Sources*, 2019, **412**, 586–596.
294 Y. Lu, Z. Hu, Y. Liu, I. Buregeya, X. Pan, N. Li and S. Chen, *Fuel Cells*, 2019, **19**, 663–674.
295 C. Gong, S. Zhao, W.-C. Tsen, F. Hu, F. Zhong, B. Zhang, H. Liu, G. Zheng, C. Qin and S. Wen, *J. Power Sources*, 2019, **441**, 227176.
296 M. L. Di Vona, M. Casciola, A. Donnadio, M. Nocchetti, L. Pasquini, R. Narducci and P. Knauth, *Int. J. Hydrogen Energy*, 2017, **42**, 3197–3205.
297 N. Chen, C. Long, Y. Li, D. Wang, C. Lu, H. Zhu and J. Yu, *ACS Appl. Mater. Interfaces*, 2018, **10**, 18246–18256.
298 D. Ion-Ebrasu, B. G. Pollet, S. Caprarescu, A. Chitu, R. Trusca, V. Niculescu, R. Gabor, E. Carcadea, M. Varlam and B. S. Vasile, *Int. J. Hydrogen Energy*, 2020, **45**, 17057–17066.
299 N. Carboni, L. Mazzapioda, A. Caprì, I. Gatto, A. Carbone, V. Baglio and M. A. Navarra, *Electrochim. Acta*, 2024, **486**, 144090.
300 G. Das, B. J. Park, J. Kim, D. Kang and H. H. Yoon, *Sci. Rep.*, 2019, **9**, 9572.
301 I. Arunkumar, A. R. Kim, S. H. Lee and D. J. Yoo, *Int. J. Hydrogen Energy*, 2024, **52**, 139–153.
302 O. Movil, L. Frank and J. A. Staser, *J. Electrochem. Soc.*, 2015, **162**, F419–F426.
303 T. Zhu, Y. Sha, H. A. Firouzjaie, X. Peng, Y. Cha, D. M. M. M. Dissanayake, M. D. Smith, A. K. Vannucci, W. E. Mustain and C. Tang, *J. Am. Chem. Soc.*, 2020, **142**, 1083–1089.
304 Z. Wang, G. Li, W. Hou, H. Guo, L. Wang and M. Wu, *ACS Nano*, 2023, **17**, 8671–8679.
305 S. Yu, P. Zhou, J. Hao and Y. Zhou, *Polymer*, 2023, **283**, 126256.
306 C. Long, C. Lu, Y. Li, Z. Wang and H. Zhu, *Int. J. Hydrogen Energy*, 2020, **45**, 19778–19790.
307 Q. Yang, C. X. Lin, F. H. Liu, L. Li, Q. G. Zhang, A. M. Zhu and Q. L. Liu, *J. Membr. Sci.*, 2018, **552**, 367–376.
308 D. Zhang, N. Ye, S. Chen, R. Wan, Y. Yang and R. He, *Renew. Energy*, 2020, **160**, 250–260.
309 H. Zarrin, J. Fu, G. Jiang, S. Yoo, J. Lenos, M. Fowler and Z. Chen, *ACS Nano*, 2015, **9**, 2028–2037.
310 J. Y. Chu, K. H. Lee, A. R. Kim and D. J. Yoo, *Compos. B Eng.*, 2019, **164**, 324–332.
311 D. Zhang, S. Xu, R. Wan, Y. Yang and R. He, *J. Power Sources*, 2022, **517**, 230720.
312 D. Shen, Y. Liu, C. Chen, Z. Yang, H. Li, S. Xiao, W. Wu and J. Wang, *Adv. Funct. Mater.*, 2025, DOI: 10.1002/adfm.202515358.
313 Y. Zheng, Y. Liu, H. Li, Z. Yang, W. Wu, J. Zhang, J. Wu and J. Wang, *Adv. Funct. Mater.*, 2025, **35**(37), DOI: 10.1002/adfm.202500151.
314 C. Wang, Z. Yang, W. Wu, C. Chen, Y. Li, R. Zhang, W. Li, K. Dai and J. Wang, *Chem. Mater.*, 2024, **36**, 8255–8263.
315 J. Ren, J. Xu, M. Ju, X. Chen, P. Zhao, L. Meng, J. Lei and Z. Wang, *Adv. Powder Mater.*, 2022, **1**, 100017.
316 Y. Lin, H. Gao, Q. Zhou, Q. Huang, M. Zhao and S. Tang, *Int. J. Hydrogen Energy*, 2025, **145**, 75–83.
317 X. Liao, L. Ren, D. Chen, X. Liu and H. Zhang, *J. Power Sources*, 2015, **286**, 258–263.

318 M. T. Pérez-Prior, T. García-García, A. Várez and B. Levenfeld, *J. Mater. Sci.*, 2015, **50**, 5893–5903.
319 S. Xu, R. Jiang, S. Jiang and Y. Gao, *J. Electrochem. Soc.*, 2016, **163**, F688–F690.
320 Y. Chen, Z. Li, N. Chen, R. Li, Y. Zhang, K. Li, F. Wang and H. Zhu, *Electrochim. Acta*, 2017, **255**, 335–346.
321 A. R. Ferrari, D. Stucchi, T. Caielli, R. Akbari, I. C. Pellini, C. Antonini and P. Mustarelli, *Solid State Ionics*, 2025, **430**, 116996.